

## Unusual Hydridicity of a Cobalt Bound Si-H Moiety

Jin Kim,<sup>a</sup> Yujeong Kim,<sup>c,d</sup> Indranil Sinha,<sup>a,b</sup> Sun Hee Kim<sup>\*,c,d</sup> and Yunho Lee<sup>\*,a,b</sup>

<sup>a</sup> Department of Chemistry, Korea Advanced Institute of Science and Technology,  
Daejeon 34141, Republic of Korea

<sup>b</sup> Centre for Catalytic Hydrocarbon Functionalizations, Institute for Basic Science,  
Daejeon, 34141, Republic of Korea

<sup>c</sup> Western Seoul Centre, Korea Basic Science Institute, Seoul 03759, Republic of Korea

<sup>d</sup> Department of Chemistry and Nano Science, Ewha Womans University, Seoul 03760, Republic of Korea

### Contents

#### Experimental Section

**Figure S1.** <sup>1</sup>H NMR spectrum of **a**.

**Figure S2.** <sup>13</sup>C NMR spectrum of **a**.

**Figure S3.** <sup>29</sup>Si NMR spectrum of **a**.

**Figure S4.** <sup>31</sup>P NMR spectrum of **a**.

**Figure S5.** <sup>1</sup>H NMR spectrum of **MeSiP<sub>2</sub>Cl**.

**Figure S6.** <sup>13</sup>C NMR spectrum of **MeSiP<sub>2</sub>Cl**.

**Figure S7.** <sup>29</sup>Si NMR spectrum of **MeSiP<sub>2</sub>Cl**.

**Figure S8.** <sup>31</sup>P NMR spectrum of **MeSiP<sub>2</sub>Cl**.

**Figure S9.** <sup>1</sup>H NMR spectrum of **b-D**.

**Figure S10.** <sup>2</sup>H NMR spectrum of **b-D**.

**Figure S11.** <sup>31</sup>P NMR spectrum of **b-D**.

**Figure S12.** <sup>1</sup>H NMR spectrum of **1a**.

**Figure S13.** <sup>1</sup>H NMR spectrum of **1b**.

**Figure S14.** X-band EPR spectrum of **1a** at 20 K.

**Figure S15.** X-band EPR spectrum of **1b** at 20 K.

**Figure S16.** X-band EPR spectrum of **2a** at 20 K.

**Figure S17.** X-band EPR spectrum of **2b** at 20 K.

**Figure S18.** X-band EPR spectrum of *in situ* sample of **3a** at 20 K.

**Figure S19.** X-band EPR spectrum of *in situ* sample of **3b** at 20 K.

**Figure S20.** X-band CW and Q-band Electron Spin Echo detected EPR spectra of **3b**.

**Figure S21.** Q-band <sup>2</sup>H Mims ENDOR spectra of **3b** and **3b-D**.

**Figure S22.** Q-band <sup>1</sup>H Davies ENDOR spectra of **3b** and **3b-D**.

**Figure S23.** Q-band three-pulse ESEEM and Mims ENDOR spectra of **3b-D**.

**Figure S24.** Q-band three-pulse ESEEM spectra of **3b** and **3b-D**.

**Figure S25.** Q-band three-pulse ESEEM spectra of **3b-D** at various fields.

**Figure S26.** Solid state molecular structure of **a**.

**Table S1.** Selected bond distances and angles for **a**.

**Figure S27.** Solid state molecular structure of **1a**.

**Table S2.** Selected bond distances and angles for **1a**.

**Figure S28.** Solid state molecular structure of **1b**.

**Table S3.** Selected bond distances and angles for **1b**.

**Figure S29.** Solid state molecular structure of **2b**.

**Table S4.** Selected bond distances and angles for **2b**.

**Figure S30.** Solid state molecular structure of **3a**.

**Table S5.** Selected bond distances and angles for **3a**.

**Figure S31.** Solid state molecular structure of **3b**.

**Table S6.** Selected bond distances and angles for **3b**.

**Figure S32.** Solid state molecular structure of [Et<sub>3</sub>NH]<sub>2</sub>[CoBr<sub>4</sub>].

**Table S7.** Selected bond distances and angles for [Et<sub>3</sub>NH]<sub>2</sub>[CoBr<sub>4</sub>].

**Table S8.** Selected bond distances and angles of **1a-b** and **3a-b**.

**Figure S33.** UV-Vis spectra of **1a** and **1b**.

**Figure S34.** UV-Vis spectra of **2a** and **2b**.

**Figure S35.** UV-Vis spectra of **3a** and its decomposition products.

**Figure S36.** UV-Vis spectra of **3b** and its decomposition products.

**Figure S37.** UV-Vis spectral changes observed in the reaction of **3b** and triethylamine.

**Figure S38.** Plots of absorbance vs. time for the reaction of **3b** to  $\{(\text{MeSiP}_2)\text{CoBr}_2\}^-$  and  $\{(\text{MeSiP}_2)\text{CoBr}_2\}^-$  to **1b**.

***pK<sub>a</sub> measurement for 3b***

**Table S9.** pK<sub>a</sub> value of **3b**.

**Figure S39.** UV-Vis spectra of **3b** with a deprotonated intermediate species at equilibrium state.

**Figure S40.** IR spectrum of **a**.

**Figure S41.** IR spectra of **b-D** and **b**.

**Figure S42.** IR spectra of **1a** and **1b**.

**Figure S43.** IR spectra of **2a** and **2b**.

**Figure S44.** IR spectra of **3b-D** and **3b**.

**Figure S45.** ESI mass data of **a**.

**Figure S46.** ESI mass data of **MeSiP<sub>2</sub>Cl**.

**Figure S47.** ESI mass data of **b-D**.

***Computational details***

**Figure S48.** Plausible reaction pathways of **1b** formation from intermediate **3b**.

**Figure S49.** A relative free energy profile for pathway 2.

**Table S10.** Selected bond indices for **1b** and **3b** from NBO analysis.

**Table S11.** Cartesian coordinates (Å) for the optimized structure of **INT1**.

**Table S12.** Cartesian coordinates (Å) for the initial structure of **INT2 (INT2\*)**.

**Table S13.** Cartesian coordinates (Å) for the optimized structure of **INT2-LS**.

**Table S14.** Cartesian coordinates (Å) for the optimized structure of **INT2-HS**.

**Table S15.** Cartesian coordinates (Å) for the optimized structure of **INT3**.

**Table S16.** Cartesian coordinates (Å) for the optimized structure of **INT4**.

## Experimental Section

*General Considerations.* All manipulations were carried out using standard Schlenk or glovebox techniques under a N<sub>2</sub> atmosphere. Unless otherwise noted, solvents were deoxygenated and dried by thoroughly sparging with Ar gas followed by passage through an activated alumina column. Non-halogenated solvents were tested with a standard purple solution of sodium benzophenone ketyl in tetrahydrofuran in order to confirm effective oxygen and moisture removal. All reagents were purchased from commercial vendors and used without further purification unless otherwise stated. (2-bromophenyl)diisopropylphosphine<sup>1</sup> and bis(2-diisopropylphosphinophenyl)methylsilane (**b**)<sup>2</sup> was prepared according to literature procedures. Elemental analyses were carried out at the KAIST Central Research Instrument Facility on a Thermo Scientific FLASH 2000 series instrument. Deuterated solvents were purchased from Cambridge Isotope Laboratories, Inc. or Euriso-top, degassed, and dried over activated 4 Å molecular sieves prior to use.

*X-ray crystallography.* The diffraction data of **a** was collected on a Bruker SMART 1000. The diffraction data of **1a**, **1b**, **2b**, **3a**, **3b** and [Et<sub>3</sub>NH]<sub>2</sub>[CoBr<sub>4</sub>] were collected on a Bruker D8 QUEST. A suitable size and quality of crystal was coated with Paratone-*N* oil and mounted on a MiTeGen MicroLoop. The data were collected with graphite-monochromated Mo K $\alpha$  radiation ( $\lambda = 0.71073$  Å) at 100 K or 120 K. Cell parameters were determined and refined by SMART program.<sup>3</sup> Data reduction was performed using SAINT software.<sup>4</sup> An empirical absorption correction was applied using the SADABS program.<sup>5</sup> The structures were solved by direct methods, and all non-hydrogen atoms were subjected to anisotropic refinement by full-matrix least squares on F<sup>2</sup> by using the SHELXTL/PC package.<sup>6</sup> Unless otherwise noted, hydrogen atoms were placed at their geometrically calculated positions and refined riding on the corresponding carbon atoms with isotropic thermal parameters.

*Spectroscopic Measurements.* Bruker 400 spectrometer was used to measure <sup>1</sup>H NMR. The chemical shifts for <sup>1</sup>H NMR spectra were quoted in part per million (ppm) referenced to residual solvent peaks. The following abbreviations were used to describe peak splitting patterns when appropriate: s = singlet, d = doublet, t = triplet, m = multiplet, dd = doublet of doublet, br s = broad singlet. Coupling constants, *J*, were reported in hertz unit (Hz). <sup>2</sup>H NMR spectrum was recorded on Bruker 400 spectrometer. <sup>2</sup>H NMR chemical shift was quoted in part per million (ppm) referenced to C<sub>6</sub>H<sub>5</sub>D impurities in internal benzene solvent. <sup>13</sup>C NMR spectra were recorded on Bruker 400 spectrometer. <sup>13</sup>C NMR chemical shifts were quoted in part per million (ppm) referenced to internal solvent peaks. <sup>29</sup>Si NMR spectra were recorded on Bruker 400 spectrometer and were decoupled by broad band proton decoupling. The chemical shifts for <sup>29</sup>Si NMR spectra were quoted in part per million (ppm) referenced to external tetramethylsilane as 0.0 ppm. <sup>31</sup>P NMR spectra were recorded on Bruker 400 spectrometer and were decoupled by broad band proton decoupling. The chemical shifts for <sup>31</sup>P NMR spectra

---

<sup>1</sup> M. Tamm, B. Dreßel, K. Baum, T. Lügger and T. Pape, *J. Organomet. Chem.*, 2003, **677**, 1.

<sup>2</sup> H. Fang, Y.-K. Choe, Y. Li and S. Shimada, *Chem. Asian J.*, 2011, **6**, 2512.

<sup>3</sup> SMART (version 5.0), *data collection software*; Bruker AXS, Inc., Madison, WI, 1998.

<sup>4</sup> SAINT (version 5.0), *data integration software*; Bruker AXS, Inc., Madison, WI, 1998.

<sup>5</sup> G. M. Sheldrick, *SADABS: program for absorption correction with the Bruker SMART system*; Universität Göttingen, Germany, 1996.

<sup>6</sup> G. M. Sheldrick, *SHELXTL (version 6.1)*, Bruker AXS, Inc., Madison, WI, 2000.

were quoted in part per million (ppm) referenced to external phosphoric acid as 0.0 ppm. Solution magnetic moments were determined by the Evans' method.<sup>7</sup> Electrospray ionization mass spectra (ESI-MS) were collected on a Thermo Finnigan (San Jose, CA, USA) LCQTM Advantage MAX quadrupole ion trap instrument, by infusing samples directly into the source using a manual method. UV-Vis spectra were measured by Agilent Cary 60 UV-Vis spectrophotometer using a 1 cm two-window quartz spectrophotometer cell sealed with a screw-cap purchased from Hellma Analytics (117.100-QS). Low temperature UV-Vis spectra were measured by Agilent Cary 60 UV-Vis spectrophotometer with a fibre optic coupler (Agilent) and a fibre optic dip probe purchased from Hellma Analytics (661.202-UV, 10 mm). For the low temperature measurement with a Cary 60 UV-Vis spectrophotometer, a heptane/N<sub>2</sub>(l) bath (−90 °C) or a acetonitrile/dry ice bath (−40 °C) was used, and the steady temperature was monitored with the type K thermocouple (Model SDT142S, SUMMIT Co. Ltd.). Air sensitive solutions were prepared in a glovebox (N<sub>2</sub> filled, Korea Kiyon) and carried out in custom-made Schlenk tubes designed for the dip probe. Infrared spectra were recorded in KBr pellet by Agilent 660-IR. Frequencies are given in reciprocal centimetres (cm<sup>−1</sup>) and only selected absorbances were reported.

*CW and Pulsed-EPR Spectroscopy.* All EPR measurements were carried out at Korea Basic Science Institute (KBSI) in Seoul, Korea. CW X-band EPR spectra of **1a**, **1b**, **2a**, **2b**, **3a** and **3b** were collected on a Bruker EMX plus 6/1 spectrometer equipped with an Oxford Instrument ESR900 liquid He cryostat using an Oxford ITC 503 temperature controller. Spectra were collected with the following experimental parameters: microwave frequency, 9.6 GHz; microwave power, 0.96 mW; modulation amplitude, 10 G; modulation frequency, 100 kHz; temperature, 20 K. The CW-EPR simulations were performed using EasySpin.<sup>8</sup> Pulsed EPR data were obtained on a Bruker Elexsys E580 spectrometer and Cryogenic temperatures were achieved with an Oxford CF-935 cryostat and Oxford ITC temperature controller. All pulsed EPR measurements were conducted at 8 K. Q-band pulsed ENDOR data were collected using an EN5107D2 resonator. Mims ENDOR were carried out using the pulse sequence,  $\pi/2$ - $\tau$ - $\pi/2$ - $T$ - $\pi/2$ -echo, with microwave pulse lengths of 32 ns and an inter-pulse time of  $\tau = 200$  ns. In this sequence, RF power is applied during the time  $T$  (20  $\mu$ s) to drive nuclear spin transitions. The repetition time was 5 ms. Pulsed ENDOR spectra were obtained using stochastic sampling for better baseline of the spectra. The ENDOR simulations were performed using the simulation code kindly provided by Professor Brian M. Hoffman at Northwestern University. Q-band three-pulse ESEEM experiments were carried out using a pulse sequence,  $\pi/2$ - $\tau$ - $\pi/2$ - $T$ - $\pi/2$ - $\tau$ -echo, with pulse length  $t_{\pi/2} = 32$  ns. The  $\tau$  value of 300 ns was fixed but  $T$  was varied with a step size of 16 ns. A four-step phase cycle was employed to eliminate unwanted echoes. The time domain spectra were baseline corrected, apodized with a Hamming window and zero-filled to 1024 points before Fourier Transformation.

**Synthesis of bis(2-diisopropylphosphinophenyl)phenylsilane (a).** To a cold solution of (2-bromophenyl) diisopropylphosphine (3.475 g, 12.72 mmol) in 40 mL of diethyl ether was added *n*-butyllithium (7.8 mL, 1.6 M in hexane, 12 mmol) dropwise at −78 °C, resulting in an immediate colour change from colourless to orange. The resulting solution was warmed and stirred for 1 hour at room temperature. After the solution was frozen, dichlorophenylsilane (1.150 g, 6.363 mmol) was added dropwise at liquid nitrogen temperature. The resulting

---

<sup>7</sup> (a) D. F. Evans, *J. Chem. Soc.*, 1959, 2003; (b) S. K. Sur, *J. Magn. Reson.*, 1989, **82**, 169.

<sup>8</sup> S. Stoll and R. D. Britt, *Phys. Chem. Chem. Phys.*, 2009, **11**, 6614.

reaction mixture was slowly warmed to room temperature and stirred for 12 hours, resulting in a pale purple solution. The reaction mixture was filtered through Celite, and all volatiles were removed under vacuum. The product bis(2-diisopropylphosphinophenyl) phenylsilane (**a**, 2.731 g, 5.543 mmol, 87%) was isolated as a pale purple crystalline solid after recrystallization of a saturated pentane solution of **a** (~130 mL) at -35 °C. <sup>1</sup>H NMR (400 MHz, C<sub>6</sub>D<sub>6</sub>) δ 7.64 – 7.62 (m, 2H, Ar-*H*), 7.43 – 7.39 (m, 4H, Ar-*H*), 7.18 – 7.15 (m, 5H, Ar-*H*), 7.03 – 6.99 (m, 2H, Ar-*H*), 6.98 (t, <sup>4</sup>J<sub>HP</sub> = 8.8 Hz, 1H, Si*H*) 2.05 – 1.97 (m, 2H, CH(CH<sub>3</sub>)<sub>2</sub>), 1.94 – 1.86 (m, 2H, CH(CH<sub>3</sub>)<sub>2</sub>), 1.10 (dd, <sup>3</sup>J<sub>HP</sub> = 14.1 Hz, <sup>3</sup>J<sub>HH</sub> = 6.9 Hz, 6H, CH(CH<sub>3</sub>)<sub>2</sub>), 1.04 (dd, <sup>3</sup>J<sub>HP</sub> = 14.2 Hz, <sup>3</sup>J<sub>HH</sub> = 7.0 Hz, 6H, CH(CH<sub>3</sub>)<sub>2</sub>), 0.92 (dd, <sup>3</sup>J<sub>HP</sub> = 12.1 Hz, <sup>3</sup>J<sub>HH</sub> = 7.0 Hz, 6H, CH(CH<sub>3</sub>)<sub>2</sub>), 0.81 (dd, <sup>3</sup>J<sub>HP</sub> = 11.5 Hz, <sup>3</sup>J<sub>HH</sub> = 7.0 Hz, 6H, CH(CH<sub>3</sub>)<sub>2</sub>). <sup>13</sup>C NMR (101 MHz, C<sub>6</sub>D<sub>6</sub>) δ 145.6 (dd, <sup>1</sup>J<sub>CP</sub> = 45.1 Hz, <sup>5</sup>J<sub>CP</sub> = 4.9 Hz, Ar-C), 144.6 (d, <sup>2</sup>J<sub>CP</sub> = 17.0 Hz, Ar-C), 138.0 (d, <sup>2</sup>J<sub>CP</sub> = 14.5 Hz, Ar-C), 136.9 (s, Ar-C), 132.3 (s, Ar-C), 132.3 (s, Ar-C), 129.2 (s, Ar-C), 129.1 (s, Ar-C), 128.2 (s, Ar-C), 128.0 (s, Ar-C), 25.6 (d, <sup>1</sup>J<sub>CP</sub> = 14.8 Hz, CH(CH<sub>3</sub>)<sub>2</sub>), 25.3 (d, <sup>1</sup>J<sub>CP</sub> = 14.6 Hz, CH(CH<sub>3</sub>)<sub>2</sub>), 20.7 – 20.4 (m, CH(CH<sub>3</sub>)<sub>2</sub>), 20.0 (d, <sup>2</sup>J<sub>CP</sub> = 10.9 Hz, CH(CH<sub>3</sub>)<sub>2</sub>). <sup>29</sup>Si NMR (79 MHz, C<sub>6</sub>D<sub>6</sub>) δ -26.7 (t, <sup>3</sup>J<sub>SiP</sub> = 23.7 Hz). <sup>31</sup>P NMR (162 MHz, C<sub>6</sub>D<sub>6</sub>) δ 1.24 (s). IR (KBr pellet, cm<sup>-1</sup>): 2165 (ν<sub>SiH</sub>). ESI-MS {M+H}<sup>+</sup>: calcd, 493.26; found, 493.26.

**Synthesis of bis(2-diisopropylphosphinophenyl)methylchlorosilane (MeSiP<sub>2</sub>Cl).** To a solution of (2-bromophenyl)diisopropylphosphine (481 mg, 1.76 mmol) in 15 mL of diethyl ether was added n-butyllithium (1.6 M in hexane, 1.1 mL, 1.8 mmol) at -78 °C with vigorous stirring, causing an immediate colour change to orange. The solution was warmed and stirred for 1 hour at room temperature. After the solution was frozen, a solution of methyltrichlorosilane (133 mg, 0.881 mmol) in 5 mL of diethyl ether was added slowly at liquid nitrogen temperature. The mixture was slowly warmed to room temperature overnight with vigorous stirring. The resulting orange suspension was filtered through Celite and volatiles were removed under vacuum to obtain sticky orange solid. The solid was dissolved in pentane (~10 mL) and cooled to -35 °C for 12 hours. The product bis(2-diisopropylphosphinophenyl)methylchlorosilane (**MeSiP<sub>2</sub>Cl**, 334 mg, 0.718 mmol, 82%) was isolated as a yellowish white solid after washing with cold pentane (-35 °C) and drying under vacuum. <sup>1</sup>H NMR (400 MHz, C<sub>6</sub>D<sub>6</sub>) δ 8.15 – 8.12 (m, 2H, Ar-*H*), 7.34 – 7.31 (m, 2H, Ar-*H*), 7.16 – 7.10 (m, 4H, Ar-*H*), 1.90 – 1.76 (m, 4H, CH(CH<sub>3</sub>)<sub>2</sub>), 1.67 (t, <sup>5</sup>J<sub>HP</sub> = 4.2 Hz, 3H, SiCH<sub>3</sub>), 1.06 (dd, <sup>3</sup>J<sub>HP</sub> = 14.1 Hz, <sup>3</sup>J<sub>HH</sub> = 7.0 Hz, 6H, CH(CH<sub>3</sub>)<sub>2</sub>), 1.00 (dd, <sup>3</sup>J<sub>HP</sub> = 13.1 Hz, <sup>3</sup>J<sub>HH</sub> = 7.0 Hz, 6H, CH(CH<sub>3</sub>)<sub>2</sub>), 0.83 – 0.76 (m, 12H, CH(CH<sub>3</sub>)<sub>2</sub>). <sup>13</sup>C NMR (101 MHz, C<sub>6</sub>D<sub>6</sub>) δ 146.7 (dd, <sup>1</sup>J<sub>CP</sub> = 44.0, <sup>5</sup>J<sub>CP</sub> = 2.4 Hz, Ar-C), 144.3 (d, <sup>2</sup>J<sub>CP</sub> = 16.8 Hz, Ar-C), 137.6 (dd, <sup>2</sup>J<sub>CP</sub> = 15.3, <sup>4</sup>J<sub>CP</sub> = 3.1 Hz, Ar-C), 132.2 (s, Ar-C), 129.5 (s, Ar-C), 128.5 (s, Ar-C), 26.1 (d, <sup>1</sup>J<sub>CP</sub> = 14.1 Hz, CH(CH<sub>3</sub>)<sub>2</sub>), 25.8 (d, <sup>1</sup>J<sub>CP</sub> = 14.1 Hz, CH(CH<sub>3</sub>)<sub>2</sub>), 21.3 (d, <sup>2</sup>J<sub>CP</sub> = 14.5 Hz, CH(CH<sub>3</sub>)<sub>2</sub>), 20.8 (d, <sup>2</sup>J<sub>CP</sub> = 12.7 Hz, CH(CH<sub>3</sub>)<sub>2</sub>), 20.6 (d, <sup>2</sup>J<sub>CP</sub> = 18.4 Hz, CH(CH<sub>3</sub>)<sub>2</sub>), 20.0 (d, <sup>2</sup>J<sub>CP</sub> = 16.0 Hz, CH(CH<sub>3</sub>)<sub>2</sub>), 12.7 (t, <sup>4</sup>J<sub>CP</sub> = 19.4 Hz, SiCH<sub>3</sub>). <sup>29</sup>Si NMR (79 MHz, C<sub>6</sub>D<sub>6</sub>) δ 8.98 (t, <sup>3</sup>J<sub>SiP</sub> = 12.2 Hz). <sup>31</sup>P NMR (162 MHz, C<sub>6</sub>D<sub>6</sub>) δ 1.28 (s). ESI-MS {M-Cl}<sup>+</sup>: calcd, 429.23; found, 429.23.

**Synthesis of bis(2-diisopropylphosphinophenyl)methylsilane-D (b-D).** To a solution of **MeSiP<sub>2</sub>Cl** (0.216 g, 0.464 mmol) in 30 mL of MeCN/THF (5/1) was added sodium borodeuteride (0.194 g, 4.63 mmol). The suspension was heated at 90 °C for 24 hours with stirring. The mixture was filtered through Celite and volatiles were removed under vacuum. After the resulting pale yellow oil was dissolved in diethyl ether (10 mL), the solution was filtered through Celite and silica. The product bis(2-diisopropylphosphino phenyl)methylsilane-D (**b-D**, 0.168 g, 0.389 mmol, 83.8%) was isolated as a pale yellow oil after all volatiles were removed under

vacuum.  $^1\text{H}$  NMR (400 MHz,  $\text{C}_6\text{D}_6$ )  $\delta$  7.74 – 7.71 (m, 2H, Ar-*H*), 7.38 – 7.35 (m, 2H, Ar-*H*), 7.20 – 7.12 (m, 4H, Ar-*H*), 2.02 – 1.86 (m, 4H,  $\text{CH}(\text{CH}_3)_2$ ), 1.10 (dd,  $J = 14.1, 7.0$  Hz, 6H,  $\text{CH}(\text{CH}_3)_2$ ), 1.09 (dd,  $J = 14.1, 6.9$  Hz, 6H,  $\text{CH}(\text{CH}_3)_2$ ), 0.93 (s, 3H,  $\text{SiCH}_3$ ), 0.90 – 0.84 (m, 12H,  $\text{CH}(\text{CH}_3)_2$ ).  $^2\text{H}$  NMR (61 MHz,  $\text{C}_6\text{H}_6$ )  $\delta$  6.29 (br s).  $^{31}\text{P}$  NMR (162 MHz,  $\text{C}_6\text{D}_6$ )  $\delta$  1.12 (s). IR (KBr pellet,  $\text{cm}^{-1}$ ) 1575 ( $\nu_{\text{SiD}}$ ). ESI-MS  $\{\text{M}+\text{H}\}^+$ : calcd, 432.25; found, 432.25.

**Synthesis of  $(\text{PhSiP}_2)\text{CoBr}$  (**1a**).** To a solution of **a** (100 mg, 0.203 mmol) in 5 mL of THF was added triethylamine (75  $\mu\text{L}$ , 0.54 mmol) and cooled to  $-35$   $^\circ\text{C}$ . To the mixture was added a solution of cobalt(II) bromide (44 mg, 0.20 mmol) in 5 mL of THF at  $-35$   $^\circ\text{C}$ , resulting in immediate colour change to green. The reaction mixture was warmed and stirred for 24 hours at room temperature, resulting in a brown solution. The mixture was filtered through Celite and all volatiles were removed under vacuum. The resulting brown solid was dissolved in benzene (5 mL) and filtered through Celite. Volatiles were removed under vacuum. The product  $(\text{PhSiP}_2)\text{CoBr}$  (**1a**, 113 mg, 0.179 mmol, 90%) was isolated as a brown powder after washing with pentane and drying under vacuum.  $^1\text{H}$  NMR (400 MHz,  $\text{C}_6\text{D}_6$ )  $\delta$  12.4, 9.93, 7.49, 6.66, 5.20, 3.03, 1.60, 0.92, 0.81,  $-6.83, -24.1$ .  $\mu_{\text{eff}}$ : 2.11  $\mu\text{B}$  ( $\text{C}_6\text{D}_6$ , 25  $^\circ\text{C}$ , Evans' method). UV-Vis [THF, nm ( $\text{L mol}^{-1} \text{cm}^{-1}$ )]: 370 (2500), 483 (830), 680 (290). Anal. Calcd. For  $\text{C}_{30}\text{H}_{41}\text{BrCoP}_2\text{Si}$ : C, 57.15; H, 6.55. Found: C, 57.36; H, 6.65. X-ray quality crystals were grown by slow diffusion of pentane into a saturated THF solution of **1a** at room temperature.

**Synthesis of  $(\text{MeSiP}_2)\text{CoBr}$  (**1b**).** To a solution of **b** (114 mg, 0.265 mmol) in 5 mL of THF was added triethylamine (110  $\mu\text{L}$ , 0.789 mmol) and cooled to  $-35$   $^\circ\text{C}$ . To the mixture was added a solution of cobalt(II) bromide (58 mg, 0.26 mmol) in 5 mL of THF at  $-35$   $^\circ\text{C}$ , resulting in immediate colour change to green. The reaction mixture was warmed and stirred for 24 hours at room temperature, resulting in a brown solution. The mixture was filtered through Celite and all volatiles were removed under vacuum. The resulting brown solid was dissolved in benzene (5 mL) and filtered through Celite. Volatiles were removed under vacuum. The product  $(\text{MeSiP}_2)\text{CoBr}$  (**1b**, 120 mg, 0.211 mmol, 81%) was isolated as a brownish red powder after washing with pentane and drying under vacuum.  $^1\text{H}$  NMR (400 MHz,  $\text{C}_6\text{D}_6$ )  $\delta$  14.6, 7.71, 5.71, 5.60, 3.30, 2.99,  $-0.68, -6.12, -25.1, -36.3$ .  $\mu_{\text{eff}}$ : 2.19  $\mu\text{B}$  ( $\text{C}_6\text{D}_6$ , 25  $^\circ\text{C}$ , Evans' method). UV-Vis [THF, nm ( $\text{L mol}^{-1} \text{cm}^{-1}$ )]: 370 (1800), 470 (660), 665 (120). Anal. Calcd. for  $\text{C}_{25}\text{H}_{39}\text{BrCoP}_2\text{Si}$ : C, 52.82; H, 6.92. Found: C, 53.03; H, 6.79. X-ray quality crystals were grown by slow diffusion of pentane into a saturated THF solution of **1b** at room temperature.

**Synthesis of  $[\text{PhSi}^{\text{H}}\text{P}^{\text{H}}_2][\text{CoBr}_4]$  (**2a**).** To a solution of **a** (96 mg, 0.20 mmol) in 5 mL of THF was added cobalt(II) bromide (43 mg, 0.19 mmol), resulting in a green solution. The mixture was stirred at room temperature for 1 hour. All volatiles were removed under vacuum. The resulting green solid was dissolved in benzene (10 mL) and filtered. The precipitates were collected and washed with benzene and diethyl ether. The product  $[\text{PhSi}^{\text{H}}\text{P}^{\text{H}}_2][\text{CoBr}_4]$  (**2a**, 39 mg, 0.045 mmol, 24%) was isolated as a pale blue powder after drying under vacuum.  $\mu_{\text{eff}}$ : 4.92  $\mu\text{B}$  ( $\text{CD}_3\text{CN}$ , 25  $^\circ\text{C}$ , Evans' method). UV-Vis [ $\text{MeCN}$ , nm ( $\text{L mol}^{-1} \text{cm}^{-1}$ )]: 304 (3900), 619 (590), 633 (510), 699 (930). IR (KBr pellet,  $\text{cm}^{-1}$ ): 2386 ( $\nu_{\text{PH}}$ ), 2165 ( $\nu_{\text{SiH}}$ ). Anal. Calcd. for  $\text{C}_{30}\text{H}_{44}\text{Br}_4\text{CoP}_2\text{Si}$ : C, 41.26; H, 5.08. Found: C, 41.62; H, 5.08.

**Synthesis of  $[\text{MeSi}^{\text{H}}\text{P}^{\text{H}}_2][\text{CoBr}_4]$  (**2b**).** To a solution of **b** (117 mg, 0.272 mmol) in 10 mL of THF was added cobalt(II) bromide (59 mg, 0.27 mmol), resulting in a green suspension. After the mixture was stirred at room temperature for 1 hour, the precipitates were filtered and collected. The product  $[\text{MeSi}^{\text{H}}\text{P}^{\text{H}}_2][\text{CoBr}_4]$  (**2b**, 40 mg,

0.049 mmol, 18%) was isolated as a pale blue powder after washing with THF and pentane and drying under vacuum.  $\mu_{\text{eff}}$ : 4.58  $\mu\text{B}$  ( $\text{CD}_3\text{CN}$ , 25 °C, Evans' method). UV-Vis [ $\text{MeCN}$ , nm ( $\text{L mol}^{-1} \text{cm}^{-1}$ )]: 304 (3200), 619 (510), 633 (450), 700 (860). IR (KBr pellet,  $\text{cm}^{-1}$ ): 2387 ( $\nu_{\text{PH}}$ ), 2180 ( $\nu_{\text{SiH}}$ ). Anal. Calcd. for  $\text{C}_{25}\text{H}_{42}\text{Br}_4\text{CoP}_2\text{Si}$ : C, 37.02; H, 5.22. Found: C, 37.23; H, 5.29. X-ray quality crystals were grown by slow diffusion of diethyl ether into a saturated acetonitrile solution of **2b** at room temperature.

**Low temperature generation of  $(\text{PhSi}^{\text{H}}\text{P}_2)\text{CoBr}_2$  (**3a**).** To a solution of cobalt(II) bromide (44 mg, 0.20 mmol) in 3 mL of THF was added a solution of **a** (95 mg, 0.19 mmol) in 1 mL of THF at  $-120$  °C, resulting in a green solution. At low temperature, the green solution was vigorously stirred for 30 minutes and filtered through Celite. UV-Vis [THF, nm ( $\text{L mol}^{-1} \text{cm}^{-1}$ ),  $-90$  °C]: 456 (180), 630 (450), 667 (460), 740 (420). X-ray quality crystals were grown by slow diffusion of pentane into a saturated THF solution of **3a** at  $-35$  °C.

**Low temperature generation of  $(\text{MeSi}^{\text{H}}\text{P}_2)\text{CoBr}_2$  (**3b**).** To a solution of cobalt(II) bromide (65 mg, 0.29 mmol) in 3 mL of THF was added a solution of **b** (106 mg, 0.246 mmol) in 1 mL of THF at  $-120$  °C, resulting in a green solution. At low temperature, the green solution was vigorously stirred for 30 minutes and filtered through Celite. After cold pentane ( $\sim 45$  mL,  $-120$  °C) was layered, the resulting solution was stored at  $-35$  °C for 1 day. A blue green powder (128 mg) was isolated after decanting the supernatant, washing with pentane and drying under vacuum. UV-Vis [THF, nm ( $\text{L mol}^{-1} \text{cm}^{-1}$ ),  $-40$  °C]: 450 (800), 630 (380), 670 (360), 740 (300). IR (KBr pellet,  $\text{cm}^{-1}$ ): 2102 ( $\nu_{\text{SiH}}$ ). X-ray quality crystals were grown by slow diffusion of pentane into a saturated THF solution of **3b** at  $-35$  °C.

**Low temperature generation of  $(\text{MeSi}^{\text{D}}\text{P}_2)\text{CoBr}_2$  (**3b-D**).** The same procedure used for **3b** was conducted using **b-D**. IR (KBr pellet,  $\text{cm}^{-1}$ ): 1527 ( $\nu_{\text{SiD}}$ ).

**EPR spectroscopic detection of  $(\text{PhSi}^{\text{H}}\text{P}_2)\text{CoBr}_2$  (**3a**).** To a solution of cobalt(II) bromide (10 mg, 0.047 mmol) in 2 mL of THF/2-MeTHF (9/1) was added a solution of **a** (23 mg, 0.047 mmol) in 3 mL of THF/2-MeTHF (9/1) at  $-120$  °C, resulting in a green solution. After 30 minutes of stirring at low temperature, the solution was filtered through Celite. Aliquots were collected to prepare samples for EPR measurements.

**EPR spectroscopic detection of  $(\text{MeSi}^{\text{H}}\text{P}_2)\text{CoBr}_2$  (**3b**).** To a solution of cobalt(II) bromide (12 mg, 0.055 mmol) in 2 mL of THF/2-MeTHF (9/1) was added a solution of **b** (24 mg, 0.056 mmol) in 3 mL of THF/2-MeTHF (9/1) at  $-120$  °C, resulting in a green solution. After 30 minutes of stirring at low temperature, the solution was filtered through Celite. Aliquots were collected to prepare samples for EPR measurements.

**Low temperature UV-Vis spectroscopic detection of  $(\text{RSi}^{\text{H}}\text{P}_2)\text{CoBr}_2$  (**3**).** To a solution of cobalt(II) bromide (2.4 mg, 0.011 mmol) in 9 mL of THF was added a solution of **a** (5.3 mg, 0.010 mmol) or **b** (4.3 mg, 0.010 mmol) in 1 mL of THF at  $-90$  °C, resulting in a pale green solution of  $(\text{PhSi}^{\text{H}}\text{P}_2)\text{CoBr}_2$  (**3a**) or  $(\text{MeSi}^{\text{H}}\text{P}_2)\text{CoBr}_2$  (**3b**). The reaction was monitored by UV-Vis spectroscopy with a variable temperature range from  $-90$  °C to room temperature.

**Reaction of  $(\text{MeSi}^{\text{H}}\text{P}_2)\text{CoBr}_2$  (**3b**) with base.** To a solution of cobalt(II) bromide (11  $\mu\text{mol}$ ) in 9 mL of THF was added a solution of **b** (10  $\mu\text{mol}$ ) in 1 mL of THF at  $-40$  °C, resulting in a pale green solution. After 5

minutes, triethylamine (130  $\mu\text{L}$ , 0.933 mmol) was added to the resulting solution of **3b**. The reaction was monitored by UV-Vis spectroscopy with a variable temperature range from  $-40\text{ }^{\circ}\text{C}$  to  $20\text{ }^{\circ}\text{C}$ .

**Kinetic experiment.** To a solution of cobalt(II) bromide (11  $\mu\text{mol}$ ) in 9 mL of THF was added a solution of **b** (10  $\mu\text{mol}$ ) in 1 mL of THF at  $-40\text{ }^{\circ}\text{C}$ , resulting in a pale green solution. After 5 minutes, an initial UV-Vis spectrum ( $300\text{ nm} < \lambda < 900\text{ nm}$ ) was measured. Triethylamine (130  $\mu\text{L}$ , 0.933 mmol) was added to the resulting solution of **3b** and spectra were collected with 20 second intervals over the course of 10 minutes at  $-40\text{ }^{\circ}\text{C}$ . The time-stacked UV-Vis spectra show the consumption of **3b** ( $\lambda_{\text{max}} = 450, 630, 670, 740\text{ nm}$ ) and an increase in new absorbance ( $\lambda_{\text{max}} = 619, 654, 688\text{ nm}$ ) indicating the formation of the deprotonated intermediate ( $\{(\text{MeSiP}_2)\text{CoBr}_2\}^-$ ). Isosbestic points were shown at  $\lambda = 650$  and  $715\text{ nm}$ . After the solution was warmed to  $20\text{ }^{\circ}\text{C}$  for 2 minutes, spectra were collected with 20 second intervals over the course of 30 minutes. The time-stacked UV-Vis spectra show the consumption of  $\{(\text{MeSiP}_2)\text{CoBr}_2\}^-$  and an increase in absorbance of **1b** ( $\lambda_{\text{max}} = 370, 470, 665\text{ nm}$ ) indicating the formation of **1b**. Isosbestic points were shown at  $\lambda = 610$  and  $715\text{ nm}$ . Absorbance at  $\lambda_{\text{max}} = 450\text{ nm}$  for reaction of **3b** and  $\lambda_{\text{max}} = 688\text{ nm}$  for  $\{(\text{MeSiP}_2)\text{CoBr}_2\}^-$  was used for plotting the absorbance vs. time and  $\ln[\mathbf{3b}$  or  $\{(\text{MeSiP}_2)\text{CoBr}_2\}^-]$  vs. time graph.

**Figure S1.**  $^1\text{H}$  NMR spectrum of bis(2-diisopropylphosphinophenyl)phenylsilane (**a**) in  $\text{C}_6\text{D}_6$ , 400 MHz at room temperature.

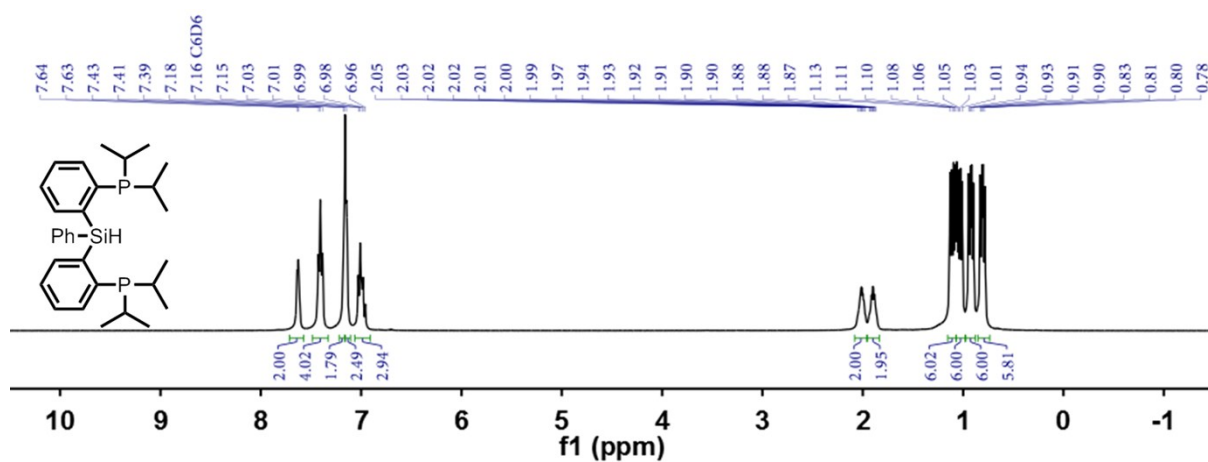


**Figure S2.**  $^{13}\text{C}$  NMR spectrum of bis(2-diisopropylphosphinophenyl)phenylsilane (**a**) in  $\text{C}_6\text{D}_6$ , 101 MHz at room temperature.

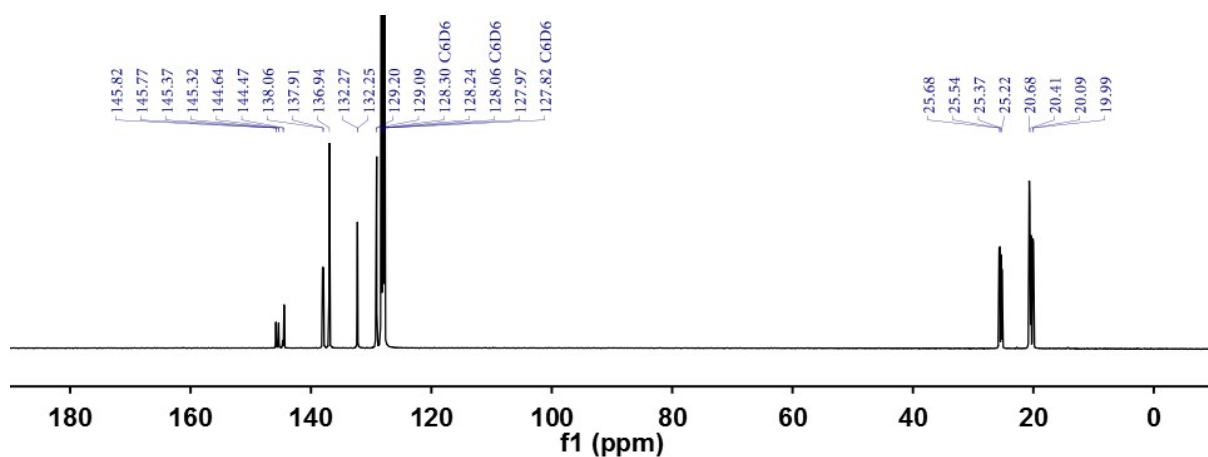


**Figure S3.**  $^{29}\text{Si}$  NMR spectrum of bis(2-diisopropylphosphinophenyl)phenylsilane (**a**) in  $\text{C}_6\text{D}_6$ , 79 MHz at room temperature.

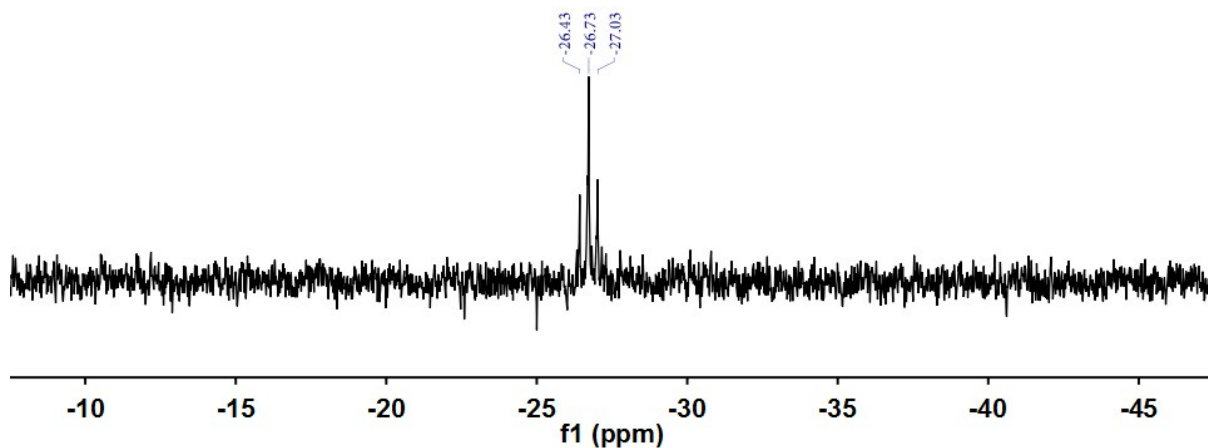


**Figure S4.**  $^{31}\text{P}$  NMR spectrum of bis(2-diisopropylphosphinophenyl)phenylsilane (**a**) in  $\text{C}_6\text{D}_6$ , 162 MHz at room temperature.

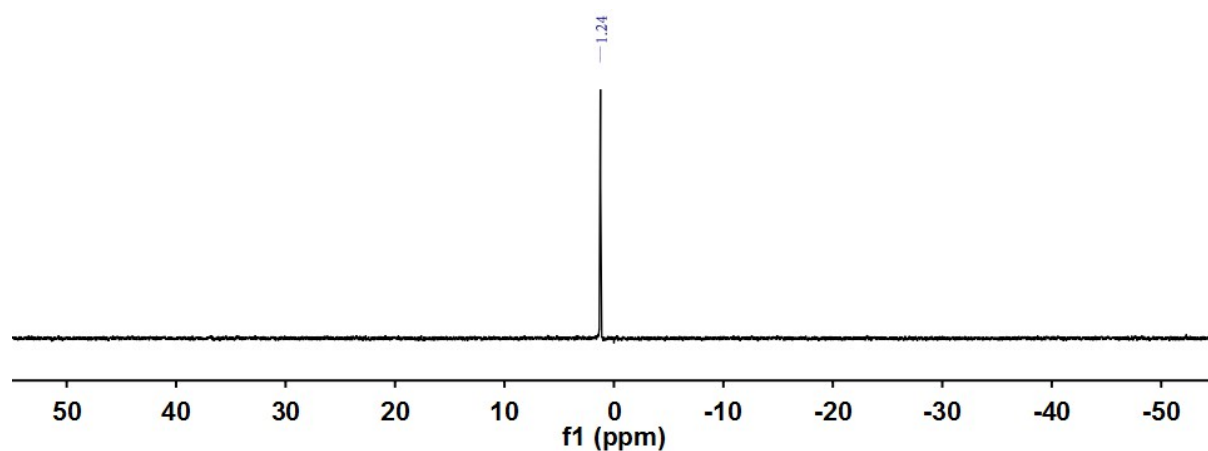


**Figure S5.**  $^1\text{H}$  NMR spectrum of bis(2-diisopropylphosphinophenyl)methylchlorosilane (**MeSiP<sub>2</sub>Cl**) in  $\text{C}_6\text{D}_6$ , 400 MHz at room temperature.

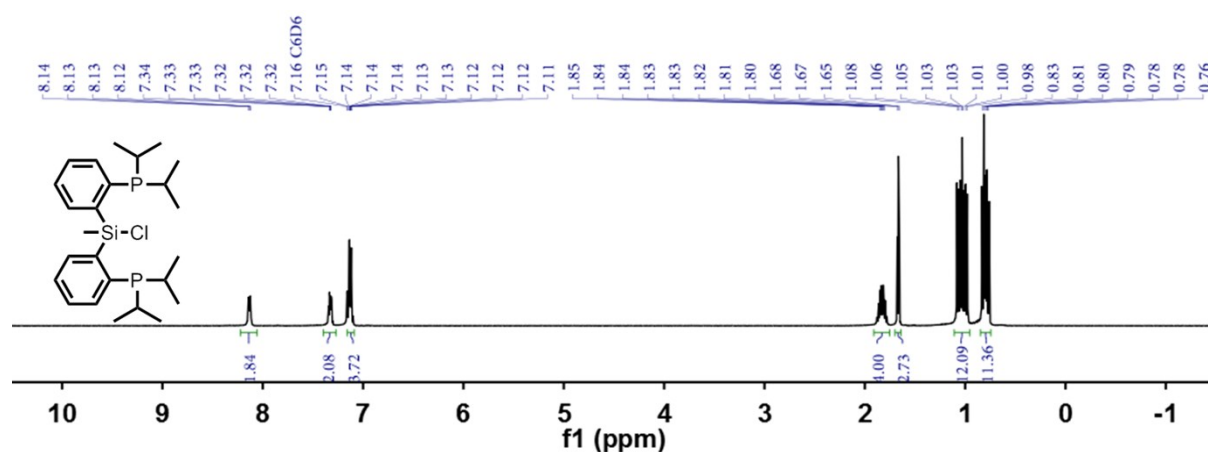


**Figure S6.**  $^{13}\text{C}$  NMR spectrum of bis(2-diisopropylphosphinophenyl)methylchlorosilane (**MeSiP<sub>2</sub>Cl**) in  $\text{C}_6\text{D}_6$ , 101 MHz at room temperature.

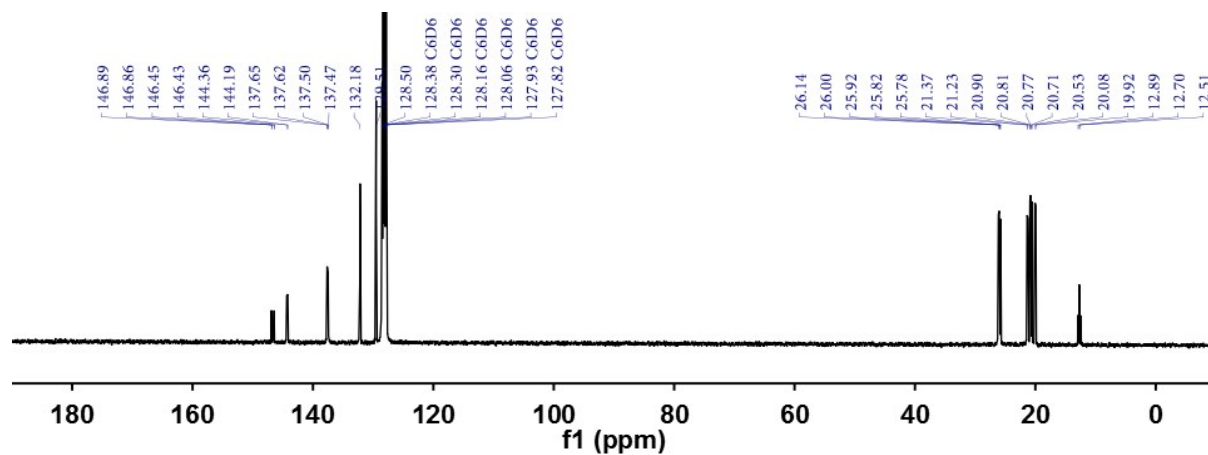


**Figure S7.**  $^{29}\text{Si}$  NMR spectrum of bis(2-diisopropylphosphinophenyl)methylchlorosilane (**MeSiP<sub>2</sub>Cl**) in  $\text{C}_6\text{D}_6$ , 79 MHz at room temperature.

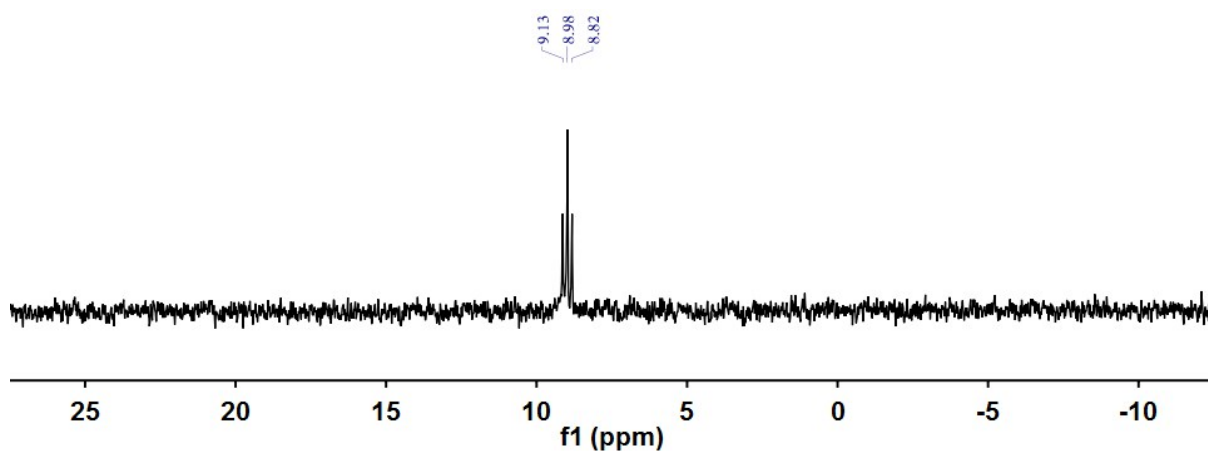


**Figure S8.**  $^{31}\text{P}$  NMR spectrum of bis(2-diisopropylphosphinophenyl)methylchlorosilane (**MeSiP<sub>2</sub>Cl**) in  $\text{C}_6\text{D}_6$ , 162 MHz at room temperature.

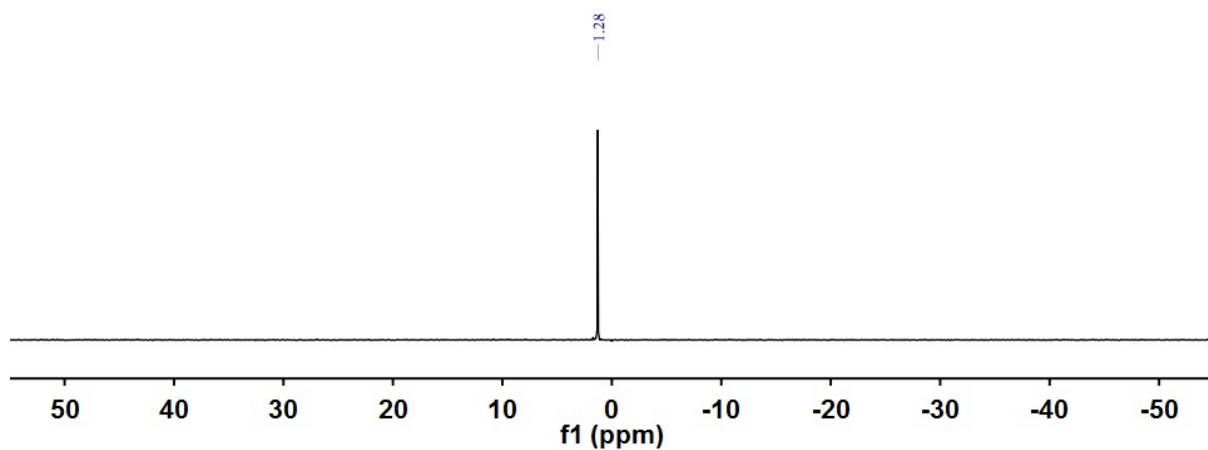


**Figure S9.**  $^1\text{H}$  NMR spectrum of bis(2-diisopropylphosphinophenyl)methylsilane-D (**b-D**) in  $\text{C}_6\text{D}_6$ , 400 MHz at room temperature.

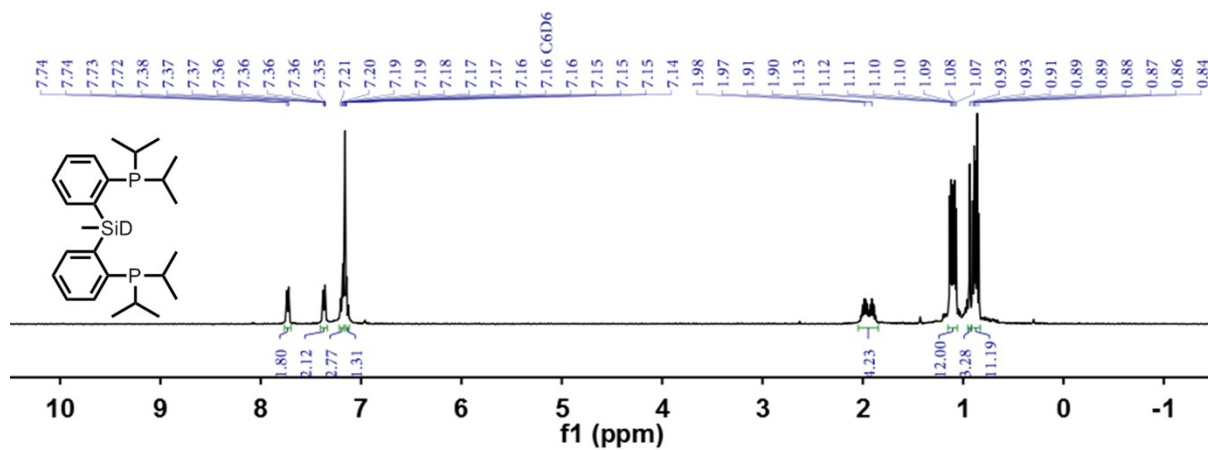


**Figure S10.**  $^2\text{H}$  NMR spectrum of bis(2-diisopropylphosphinophenyl)methylsilane-D (**b-D**) in  $\text{C}_6\text{H}_6$ , 61 MHz at room temperature.

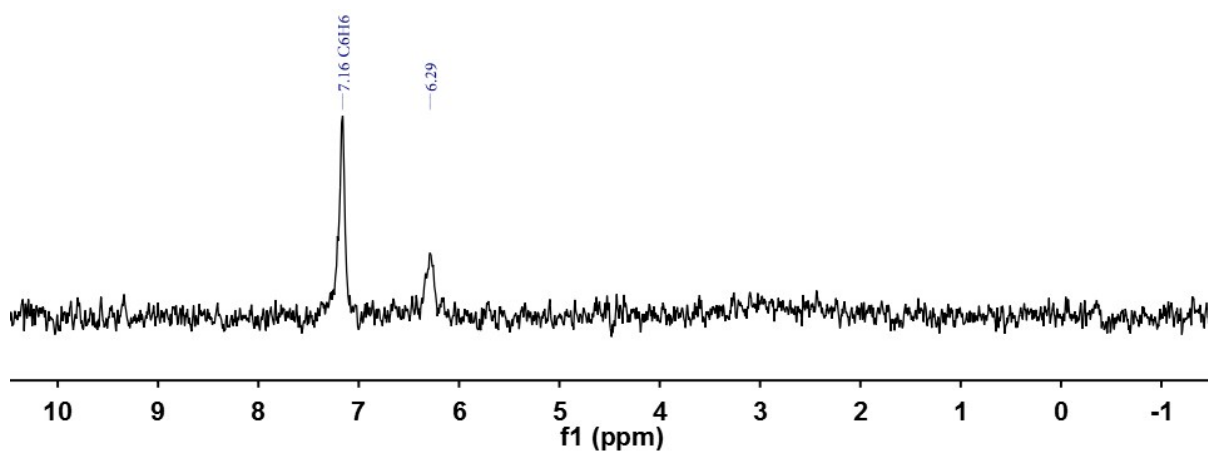


**Figure S11.**  $^{31}\text{P}$  NMR spectrum of bis(2-diisopropylphosphinophenyl)methylsilane-D (**b-D**) in  $\text{C}_6\text{D}_6$ , 162 MHz at room temperature.

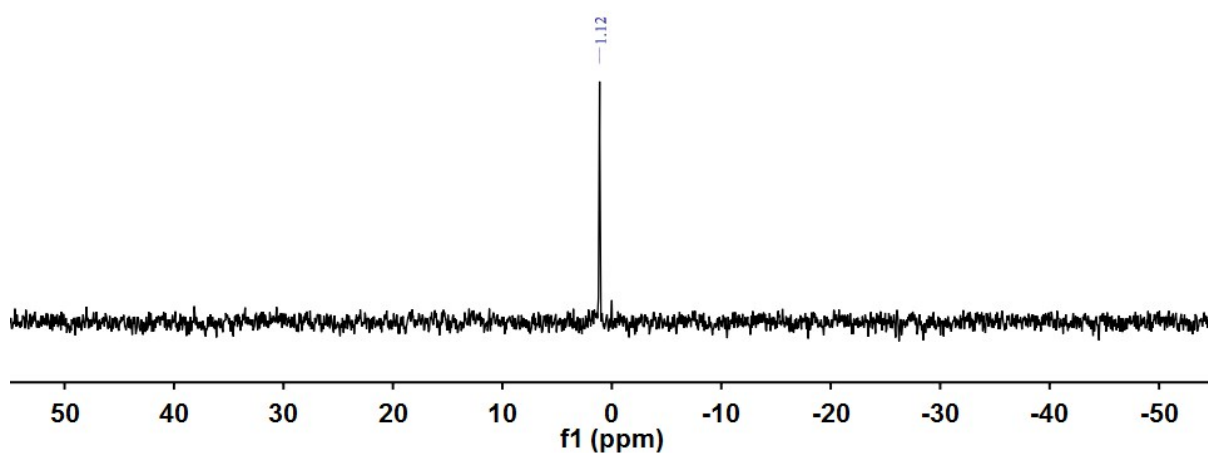


**Figure S12.**  $^1\text{H}$  NMR spectrum of  $(\text{PhSiP}_2)\text{CoBr}$  (**1a**) in  $\text{C}_6\text{D}_6$ , 400 MHz at room temperature.

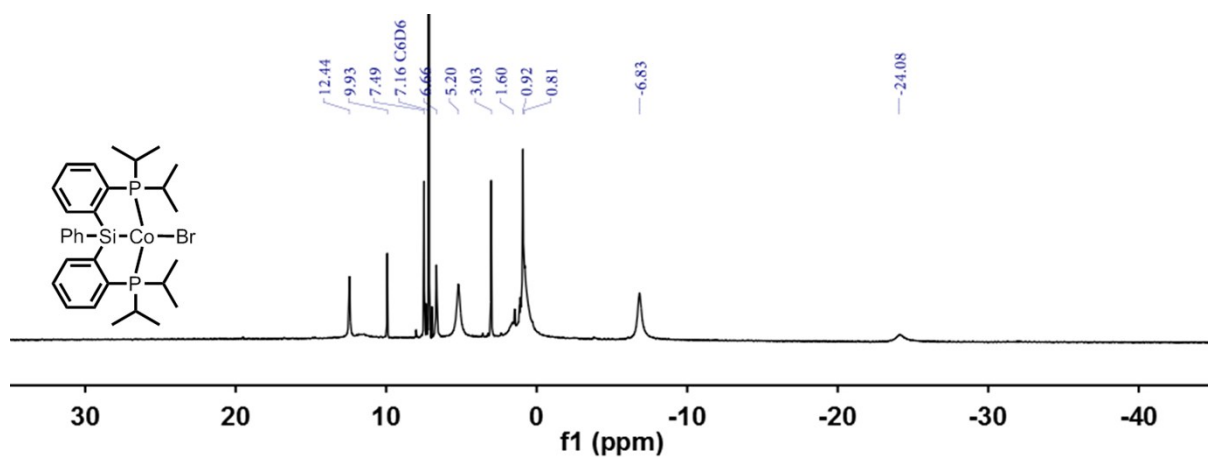
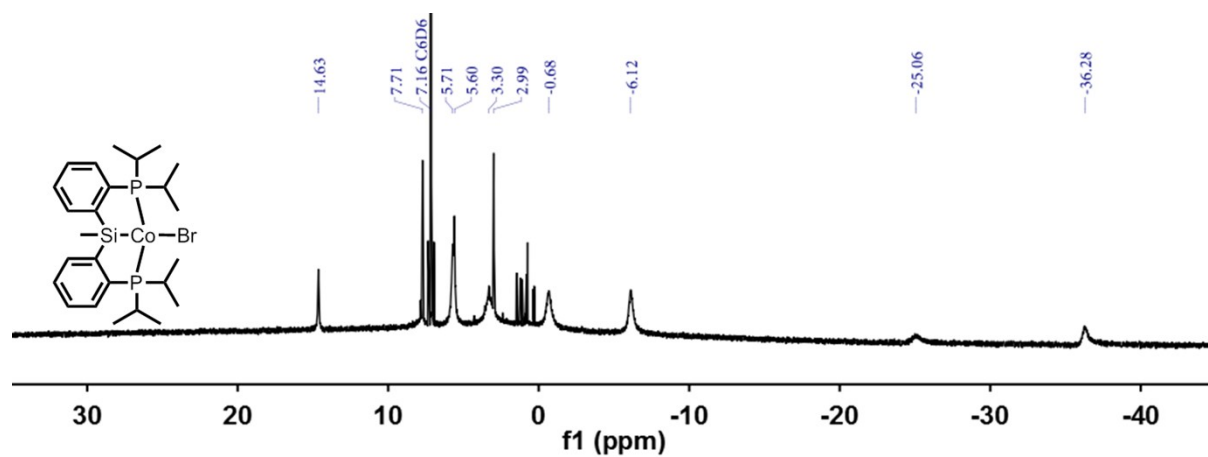
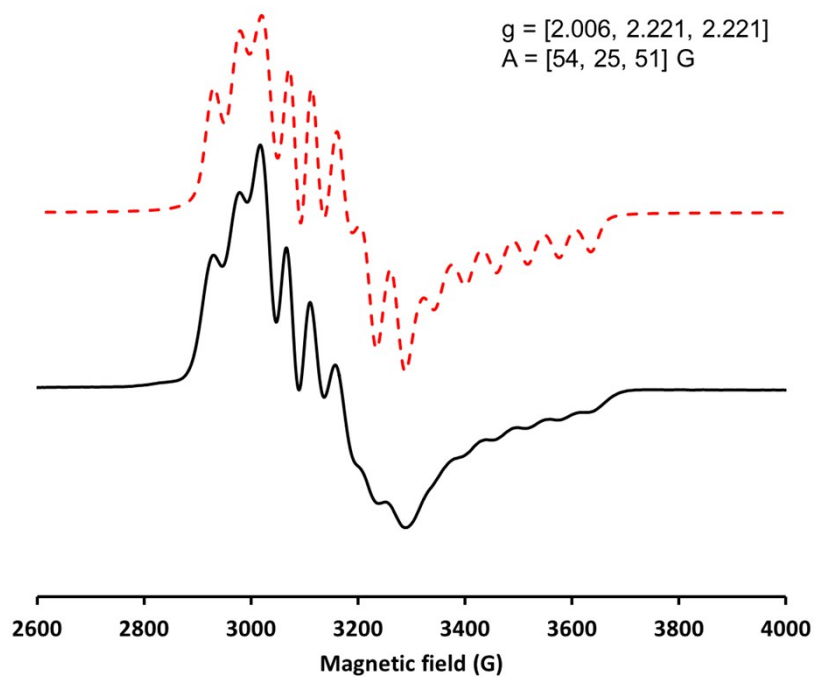


Figure S13.  $^1\text{H}$  NMR spectrum of  $(\text{MeSiP}_2)\text{CoBr}$  (**1b**) in  $\text{C}_6\text{D}_6$ , 400 MHz at room temperature.



**Figure S14.** Experimental (black line) and simulated (dashed red line) X-band EPR spectra of (PhSiP<sub>2</sub>)CoBr (**1a**) in THF/2-MeTHF (9/1) at 20 K.



**Figure S15.** Experimental (black line) and simulated (dashed red line) X-band EPR spectra of (MeSiP<sub>2</sub>)CoBr (**1b**) in THF/2-MeTHF (9/1) at 20 K.

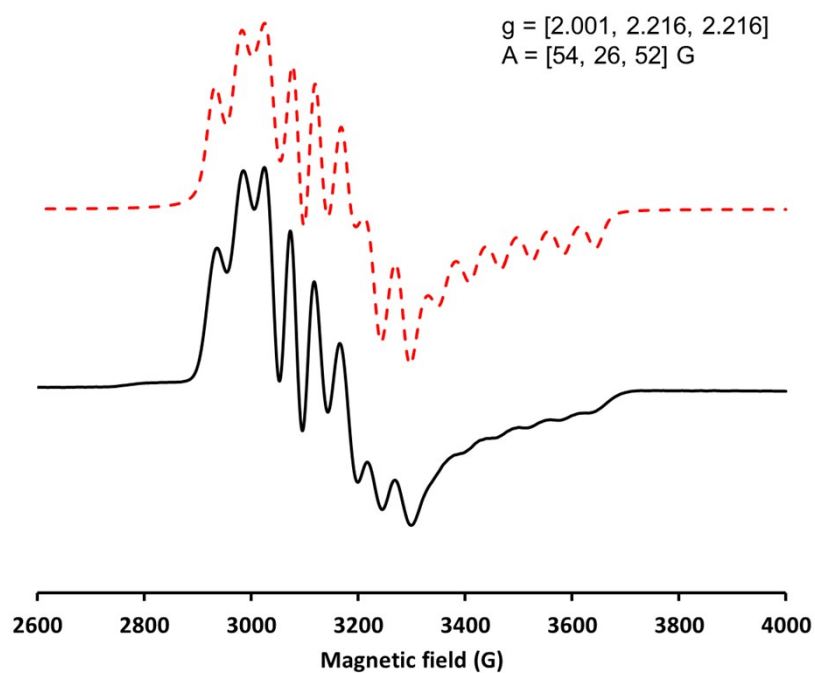


**Figure S16.** X-band EPR spectrum of  $[\text{PhSi}^{\text{H}}\text{P}^{\text{H}_2}][\text{CoBr}_4]$  (**2a**) in MeCN/DMF (1/1) at 20 K.

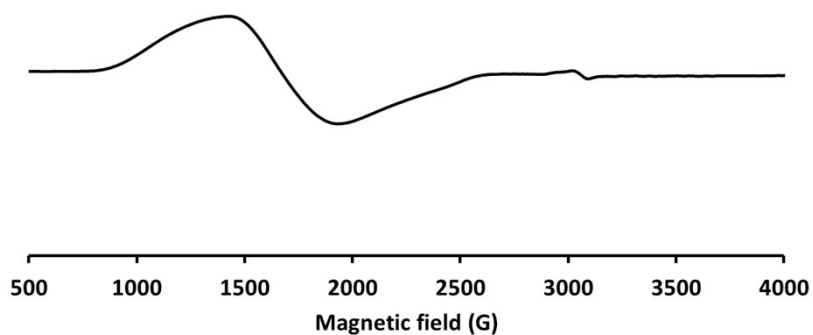


**Figure S17.** X-band EPR spectrum of  $[\text{MeSi}^{\text{H}}\text{P}^{\text{H}_2}][\text{CoBr}_4]$  (**2b**) in MeCN/DMF (1/1) at 20 K.

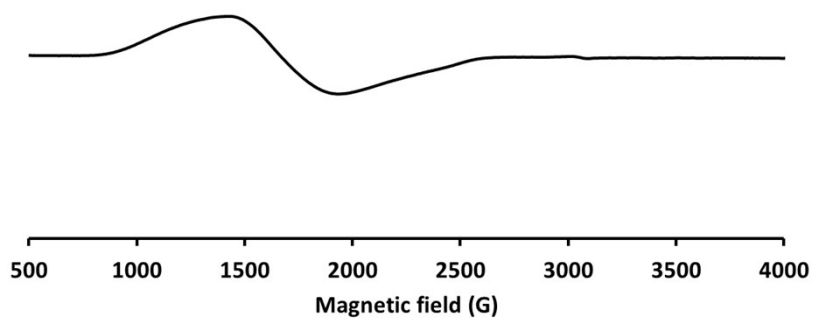


**Figure S18.** X-band EPR spectrum of *in situ* sample of  $(\text{PhSi}^{\text{H}}\text{P}_2)\text{CoBr}_2$  (**3a**) generated from the reaction of **a** and  $\text{CoBr}_2$  in THF/2-MeTHF (9/1) at  $-120\text{ }^\circ\text{C}$ , collected at 20 K.

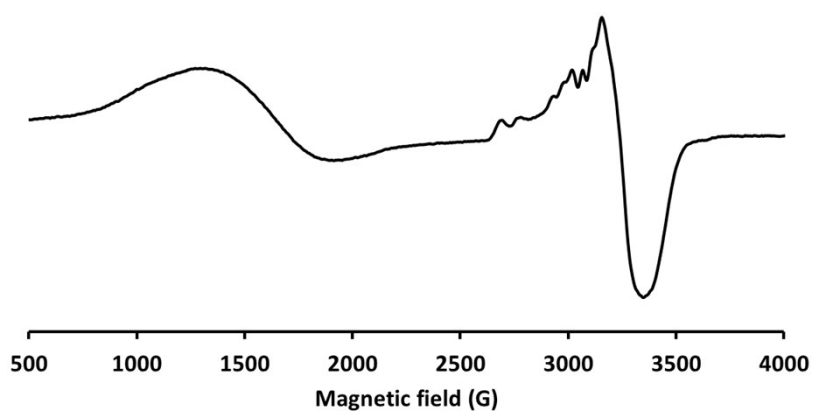


**Figure S19.** X-band EPR spectrum of *in situ* sample of  $(\text{MeSi}^{\text{H}}\text{P}_2)\text{CoBr}_2$  (**3b**) generated from the reaction of **b** and  $\text{CoBr}_2$  in THF/2-MeTHF (9/1) at  $-120^\circ\text{C}$ , collected at 20 K.

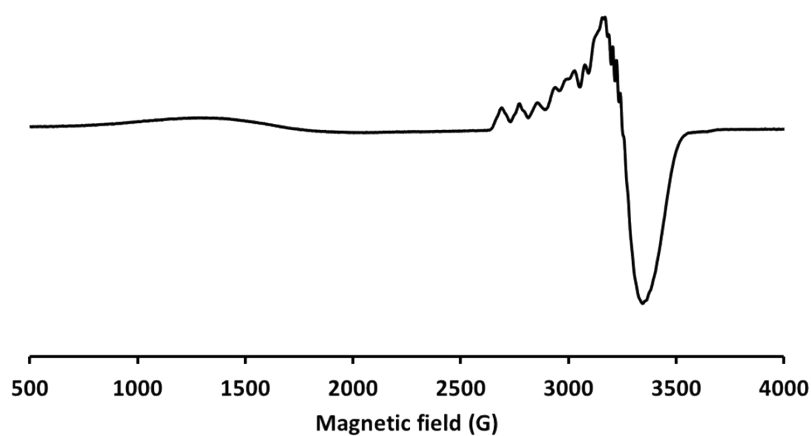


**Figure S20.** Experimental (black line) and simulated (dashed red line) (a) X-band CW-EPR and (b) Q-band Electron Spin Echo detected EPR spectra of  $(\text{MeSi}^{\text{H}}\text{P}_2)\text{CoBr}_2$  (**3b**) in THF/2-MeTHF (9/1) at  $-120^\circ\text{C}$ . Experimental Conditions: (a)  $T = 20$  K, microwave frequency = 9.64 GHz, microwave power = 0.94 mW, modulation amplitude = 10 G, modulation frequency = 100 kHz. (b)  $T = 8$  K, microwave frequency = 33.9 GHz,  $\pi/2$  pulse width = 32 ns,  $\tau = 400$  ns. Simulation parameters:  $g = [2.310, 2.145, 2.045]$ ,  $A = [90, 10, 13]$  G.

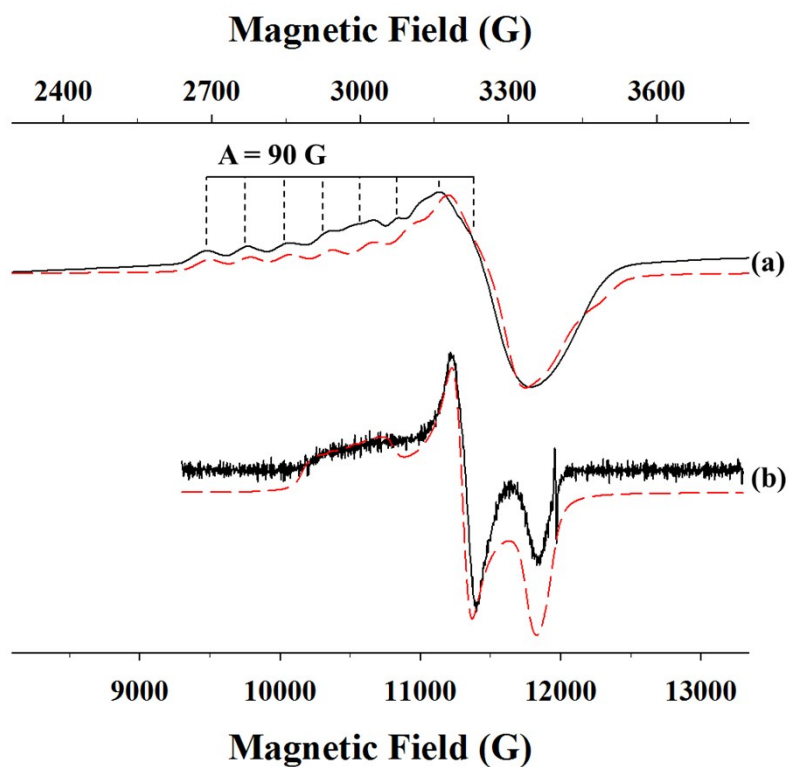


**Figure S21.** Q-band  $^2\text{H}$  Mims ENDOR spectra of (a)  $(\text{MeSi}^{\text{H}}\text{P}_2)\text{CoBr}_2$  (**3b**) and (b)  $(\text{MeSi}^{\text{D}}\text{P}_2)\text{CoBr}_2$  (**3b-D**). Experimental conditions: microwave frequency = 33.9 GHz,  $\pi/2 = 32$  ns,  $\tau = 200$  ns, RF = 20  $\mu\text{s}$ ,  $T = 8$  K, magnetic field = 10490 G. Experimental conditions: microwave frequency = 33.9 GHz,  $\pi/2 = 32$  ns,  $\tau = 200$  ns, RF = 20  $\mu\text{s}$ , magnetic field = 10820 G,  $T = 8$  K.

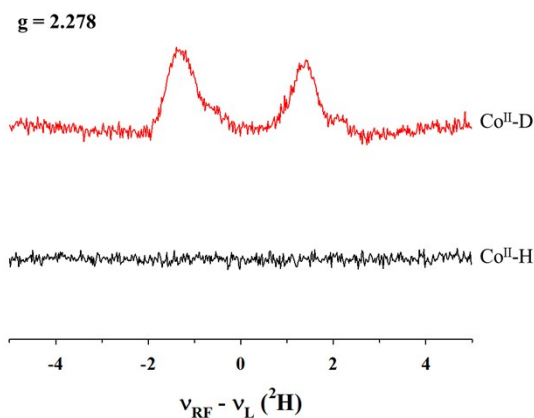


**Figure S22.** Q-band  $^1\text{H}$  Davies ENDOR spectra of (a)  $(\text{MeSi}^{\text{H}}\text{P}_2)\text{CoBr}_2$  (**3b**) and (b)  $(\text{MeSi}^{\text{D}}\text{P}_2)\text{CoBr}_2$  (**3b-D**). (c) Subtracted spectrum (a) – (b). (d)  $^2\text{H}$  Mims ENDOR of **3b-D**. Experimental conditions: microwave frequency = 33.9 GHz,  $\pi = 64$  ns,  $\pi/2 = 32$  ns,  $\tau = 200$  ns, RF = 20  $\mu\text{s}$ , magnetic field = 10490 G,  $T = 8$  K.

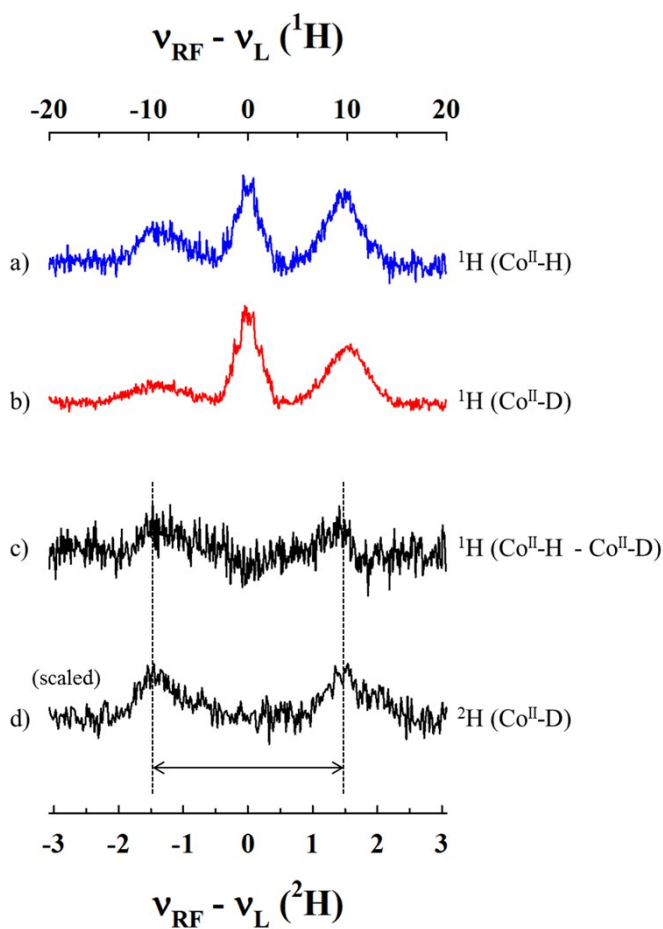


**Figure S23.** Q-band three-pulse ESEEM (black line) and Mims ENDOR (red line) spectra of **3b-D**. Experimental conditions: microwave frequency = 33.9 GHz,  $\pi/2 = 32$  ns,  $\tau = 300$  ns, initial T = 70 ns, T increment = 16 ns, S.R.T. = 2 ms  $T = 8$  K (three-pulse ESEEM) microwave frequency = 33.9 GHz,  $\pi/2 = 32$  ns,  $\tau = 200$  ns, R.F. = 20  $\mu$ s, S.R.T. = 5 ms,  $T = 8$  K (Mims ENDOR).

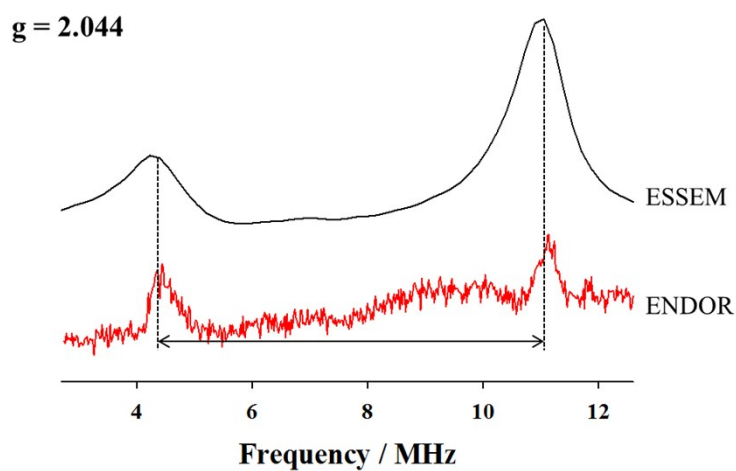
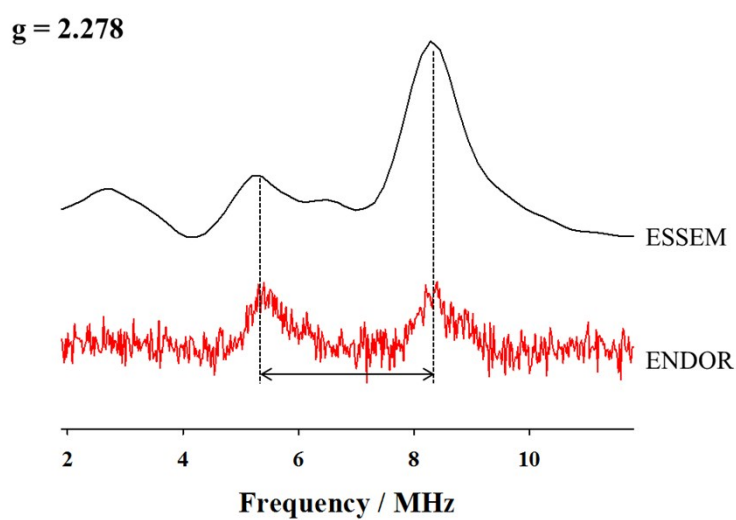


**Figure S24.** Time domain (upper) and frequency domain (bottom) Q-band three-pulse ESEEM spectra of **3b** (black line) and **3b-D** (red line). Experimental conditions: microwave frequency = 33.9 GHz,  $\pi/2 = 32$  ns,  $\tau = 300$  ns, initial  $T = 70$  ns,  $T$  increment = 16 ns, magnetic field = 11844 G,  $T = 8$  K.

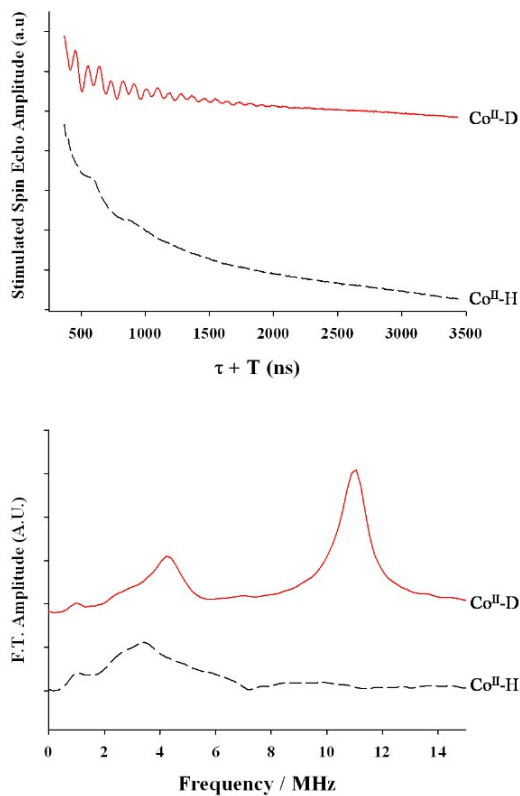


**Figure S25.** Experimental (black line) time domain (left) and frequency domain (right) Q-band three-pulse ESEEM spectra of **3b-D** at various fields and their simulated data (red dashed line). Experimental conditions: microwave frequency = 33.9 GHz,  $\pi/2 = 32$  ns,  $\tau = 300$  ns, initial  $T = 70$  ns,  $T$  increment 16 ns,  $T = 8$  K.

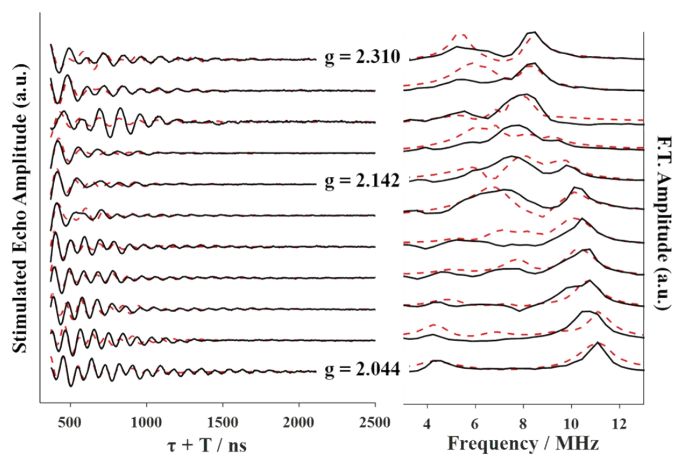




**Figure S27.** Solid state molecular structure of **1a**. All hydrogen atoms are omitted for clarity.

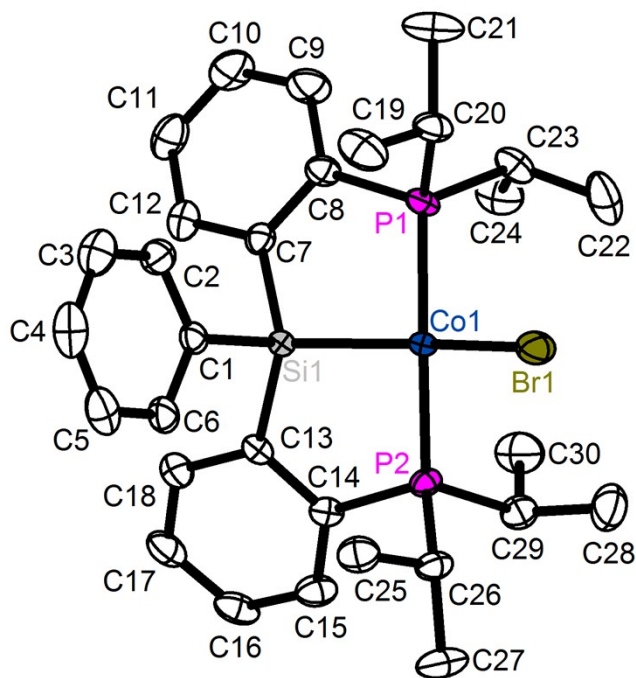


**Table S2.** Selected bond distances and angles for **1a** (Å and °).

Distance	(PhSiP <sub>2</sub> )CoBr	Angle	(PhSiP <sub>2</sub> )CoBr
d <sub>Co1-P1</sub>	2.2194(6)	∠P1-Co1-P2	144.08(3)
d <sub>Co1-P2</sub>	2.2113(6)	∠P1-Co1-Br1	102.56(2)
d <sub>Co1-Br1</sub>	2.3483(4)	∠P2-Co1-Br1	101.62(2)
d <sub>Co1-Si1</sub>	2.2437(7)	∠Si1-Co1-Br1	154.24(2)
		∠Si1-Co1-P1	84.54(2)
		∠Si1-Co1-P2	85.11(2)

**Figure S28.** Solid state molecular structure of **1b**. All hydrogen atoms are omitted for clarity.

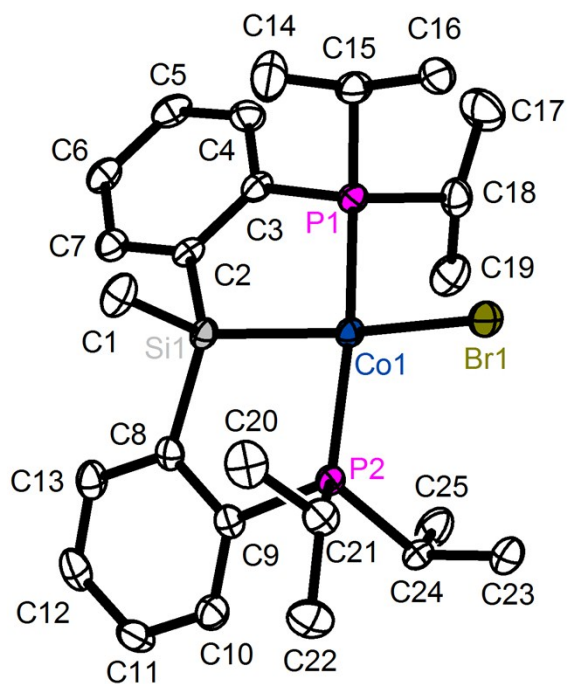


**Table S3.** Selected bond distances and angles for **1b** (Å and °).

Distance	(MeSiP <sub>2</sub> )CoBr	Angle	(MeSiP <sub>2</sub> )CoBr
d <sub>Co1-P1</sub>	2.2247(6)	∠P1-Co1-P2	159.25(3)
d <sub>Co1-P2</sub>	2.2378(6)	∠P1-Co1-Br1	96.99(2)
		∠P2-Co1-Br1	99.04(2)
d <sub>Co1-Br1</sub>	2.4045(4)	∠Si1-Co1-Br1	162.05(2)
d <sub>Co1-Si1</sub>	2.2509(6)	∠Si1-Co1-P1	84.27(2)
		∠Si1-Co1-P2	84.54(2)

**Figure S29.** Solid state molecular structure of **2b**. All hydrogen atoms except P–Hs and Si–H are omitted for clarity. P–H and Si–H hydrogen atoms were located on the Fourier difference map and their positions were freely refined.

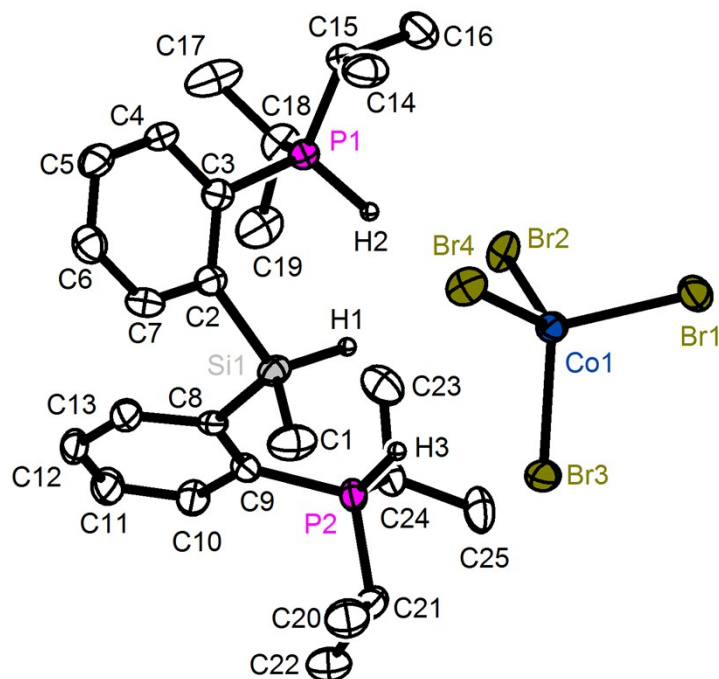


**Table S4.** Selected bond distances and angles for **2b** (Å and °).

Distance	[MeSi <sup>H</sup> P <sup>H</sup> <sub>2</sub> ][CoBr <sub>4</sub> ]	Angle	[MeSi <sup>H</sup> P <sup>H</sup> <sub>2</sub> ][CoBr <sub>4</sub> ]
d <sub>Co1–Br1</sub>	2.4031(6)	∠Br1–Co1–Br2	109.94(2)
d <sub>Co1–Br2</sub>	2.4396(6)	∠Br1–Co1–Br3	108.07(2)
		∠Br1–Co1–Br4	109.71(2)
d <sub>Co1–Br3</sub>	2.4214(6)	∠Br2–Co1–Br3	109.71(2)
		∠Br2–Co1–Br4	108.19(2)
d <sub>Co1–Br4</sub>	2.4166(6)	∠Br3–Co1–Br4	111.22(2)

**Figure S30.** Solid state molecular structure of (PhSi<sup>H</sup>P<sub>2</sub>)CoBr<sub>2</sub> (**3a**). All hydrogen atoms are omitted for clarity.

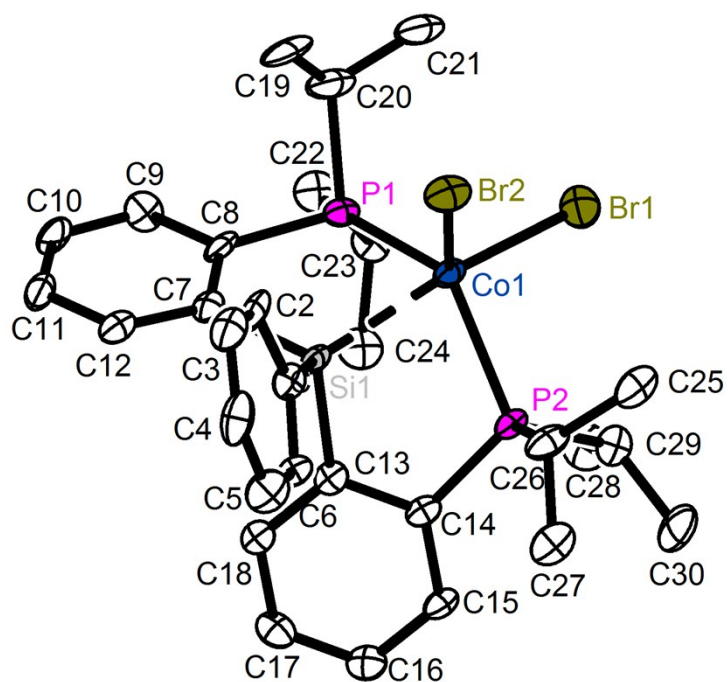


**Table S5.** Selected bond distances and angles for (PhSi<sup>H</sup>P<sub>2</sub>)CoBr<sub>2</sub> (**3a**) (Å and °).

Distance	(PhSi <sup>H</sup> P <sub>2</sub> )CoBr <sub>2</sub>	Angle	(PhSi <sup>H</sup> P <sub>2</sub> )CoBr <sub>2</sub>
d <sub>Co1-P1</sub>	2.319(3)	∠P1-Co1-P2	130.3(1)
d <sub>Co1-P2</sub>	2.342(3)	∠P1-Co1-Br1	93.7(1)
		∠P2-Co1-Br1	96.20(9)
d <sub>Co1-Br1</sub>	2.386(2)	∠P1-Co1-Si1	80.1(1)
		∠P2-Co1-Si1	78.7(1)
d <sub>Co1-Br2</sub>	2.386(2)	∠P1-Co1-Br2	112.37(9)
		∠P2-Co1-Br2	112.03(9)
d <sub>Co1-Si1</sub>	2.368(3)	∠Si1-Co1-Br1	165.9(1)
		∠Si1-Co1-Br2	89.98(9)

**Figure S31.** Solid state molecular structure of **3b**. All hydrogen atoms are omitted for clarity.

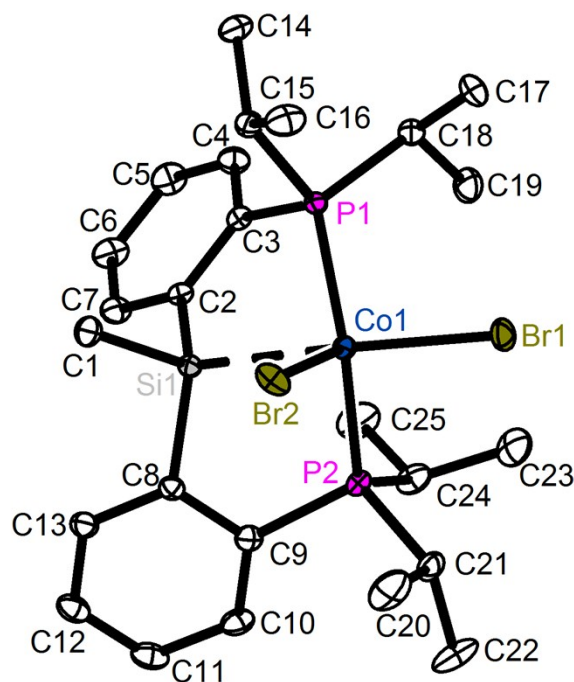


**Table S6.** Selected bond distances and angles for **3b** (Å and °).

Distance	(MeSi <sup>H</sup> P <sub>2</sub> )CoBr <sub>2</sub>	Angle	(MeSi <sup>H</sup> P <sub>2</sub> )CoBr <sub>2</sub>
d <sub>Co1-P1</sub>	2.3379(6)	∠P1-Co1-P2	123.26(2)
d <sub>Co1-P2</sub>	2.3611(7)	∠P1-Co1-Br1	100.74(2)
		∠P2-Co1-Br1	95.66(2)
d <sub>Co1-Br1</sub>	2.3718(4)	∠P1-Co1-Si1	79.62(2)
		∠P2-Co1-Si1	80.54(2)
d <sub>Co1-Br2</sub>	2.4164(4)	∠P1-Co1-Br2	116.66(2)
		∠P2-Co1-Br2	110.95(2)
d <sub>Co1-Si1</sub>	2.3652(7)	∠Si1-Co1-Br1	175.55(2)
		∠Si1-Co1-Br2	79.48(2)

**Figure S32.** Solid state molecular structure of  $[\text{Et}_3\text{NH}]_2[\text{CoBr}_4]$ . All hydrogen atoms except N–Hs are omitted for clarity. N–H hydrogen atoms were located on the Fourier difference map and their positions were freely refined.

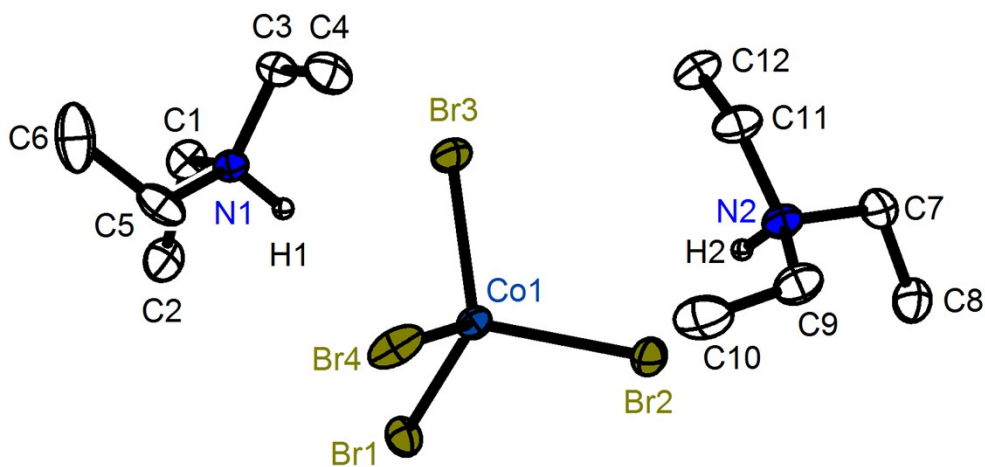


**Table S7.** Selected bond distances and angles for  $[\text{Et}_3\text{NH}]_2[\text{CoBr}_4]$  (Å and °).

Distance	$[\text{Et}_3\text{NH}]_2[\text{CoBr}_4]$	Angle	$[\text{Et}_3\text{NH}]_2[\text{CoBr}_4]$
$d_{\text{Co1}-\text{Br1}}$	2.3979(7)	$\angle\text{Br1}-\text{Co1}-\text{Br2}$	107.16(3)
$d_{\text{Co1}-\text{Br2}}$	2.4324(7)	$\angle\text{Br1}-\text{Co1}-\text{Br3}$	112.77(3)
		$\angle\text{Br1}-\text{Co1}-\text{Br4}$	108.34(3)
$d_{\text{Co1}-\text{Br3}}$	2.3968(7)	$\angle\text{Br2}-\text{Co1}-\text{Br3}$	108.59(3)
		$\angle\text{Br2}-\text{Co1}-\text{Br4}$	111.72(3)
$d_{\text{Co1}-\text{Br4}}$	2.4241(7)	$\angle\text{Br3}-\text{Co1}-\text{Br4}$	108.31(3)

**Table S8.** Selected bond distances and angles of **1a-b** and **3a-b**.

	Co–Si (Å)	Co–Br (Å)	Co–P (Å)	Si–Co–Br (deg)	P–Co–P (deg)
(PhSiP <sub>2</sub> )CoBr ( <b>1a</b> )	2.2437(7)	2.3483(4)	2.2194(6) 2.2113(6)	154.24(2)	144.08(3)
(MeSiP <sub>2</sub> )CoBr ( <b>1b</b> )	2.2509(6)	2.4045(4)	2.2247(6) 2.2378(6)	162.05(2)	159.25(3)
(PhSi <sup>H</sup> P <sub>2</sub> )CoBr <sub>2</sub> ( <b>3a</b> )	2.368(3)	2.386(2) <sup>a</sup> 2.386(2) <sup>b</sup>	2.319(3) 2.342(3)	165.9(1) <sup>c</sup> 89.98(9) <sup>d</sup>	130.3(1)
(MeSi <sup>H</sup> P <sub>2</sub> )CoBr <sub>2</sub> ( <b>3b</b> )	2.3652(7)	2.3718(4) <sup>a</sup> 2.4164(4) <sup>b</sup>	2.3379(6) 2.3611(7)	175.55(2) <sup>c</sup> 79.48(2) <sup>d</sup>	123.26(2)

<sup>a</sup>Distance for Co1–Br1. <sup>b</sup>Distance for Co1–Br2. <sup>c</sup>Angle for Si1–Co1–Br1. <sup>d</sup>Angle for Si1–Co1–Br2.

**Figure S33.** UV-Vis spectra of **1a** (red line) and **1b** (blue line) in THF at room temperature.

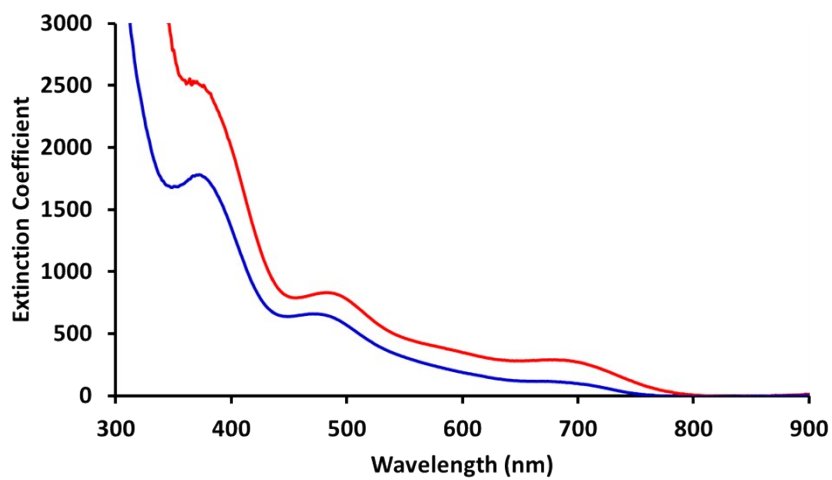


**Figure S34.** UV-Vis spectra of **2a** (red line) and **2b** (blue line) in acetonitrile at room temperature.

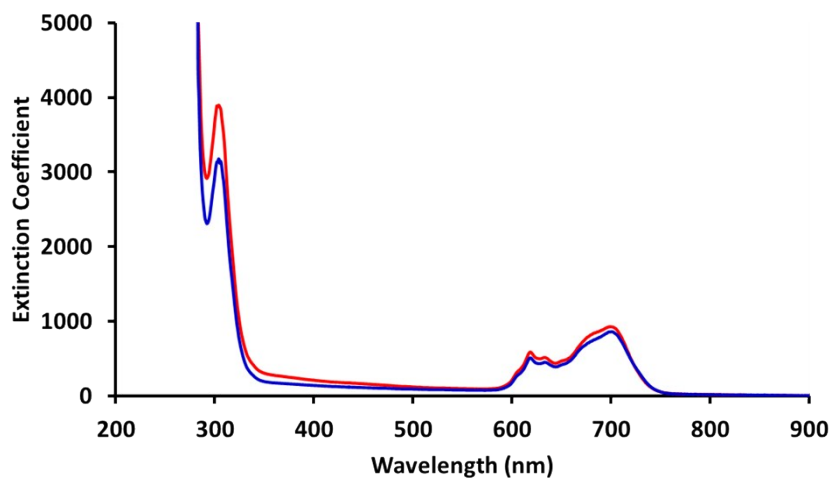


**Figure S35.** UV-Vis spectra of (a) *in situ* generated **3a** (1.0 mM in THF) from the reaction of **a** and CoBr<sub>2</sub> at –90 °C (green line, the spectrum was measured at 25 minutes after mixing) and (b) decomposed **3a** at room temperature (red line). UV-Vis spectra of (c) **1a** (dotted brown line, THF) and (d) **2a** (dotted blue line, MeCN).

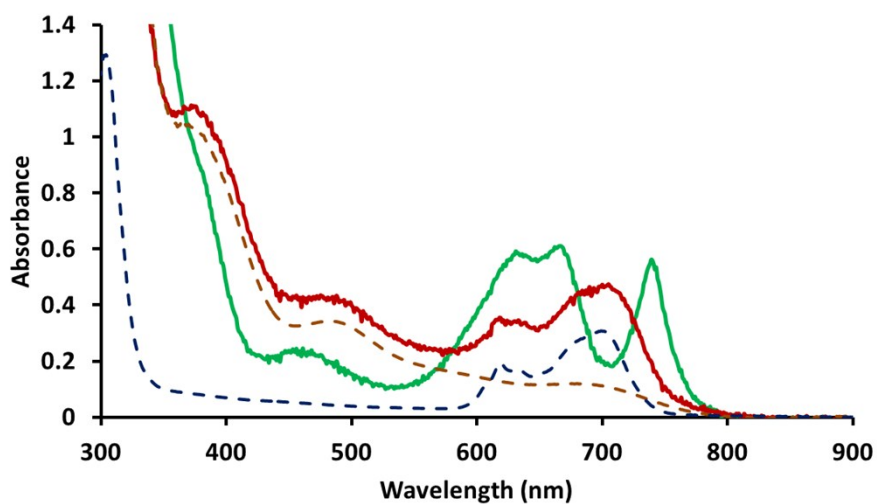


**Figure S36.** UV-Vis spectra of (a) *in situ* generated **3b** from the reaction of **b** and CoBr<sub>2</sub> at –90 °C (yellow line, the spectrum was measured at 25 minutes after mixing), (b) fully generated **3b** (1.0 mM in THF) at –40 °C (green line, the spectrum was measured after 5 minutes) and (c) decomposed **3b** at room temperature (red line). UV-Vis spectra of (d) pure **1b** (dotted brown line, THF) and (e) pure **2b** (dotted blue line, MeCN).

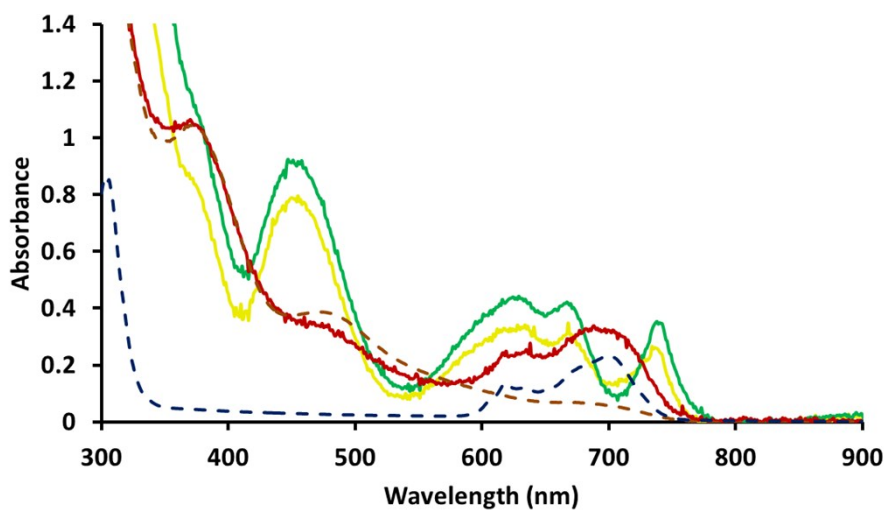


**Figure S37.** UV-Vis spectral changes observed in the reaction of **3b** and triethylamine in THF revealing (a) the formation of an intermediate species (red line) measured at  $-40\text{ }^{\circ}\text{C}$  and (b) its thermal decomposition to **1b** (blue line, with **2b** as a minor side product) measured at  $20\text{ }^{\circ}\text{C}$ .

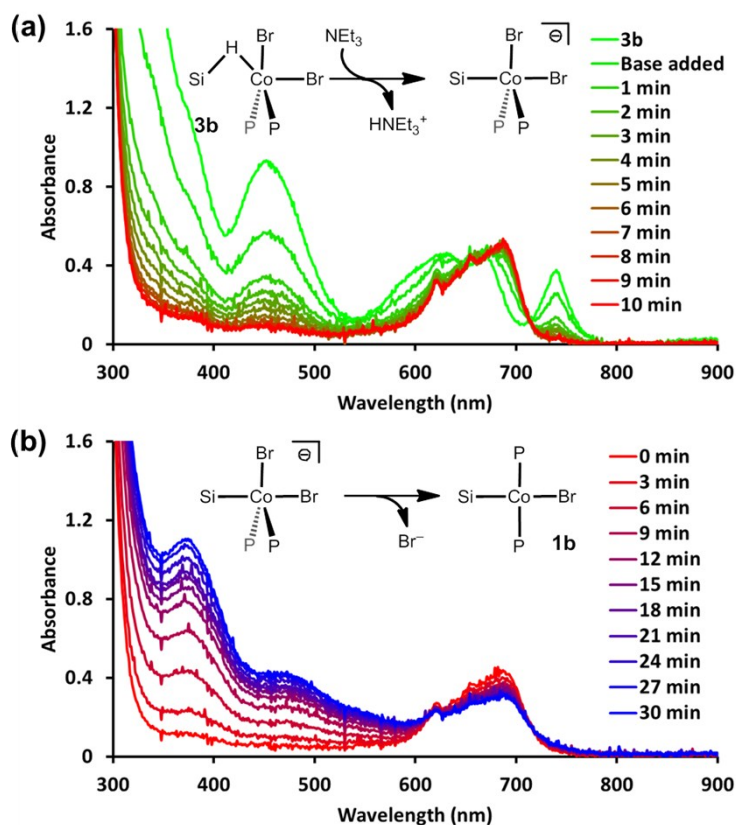
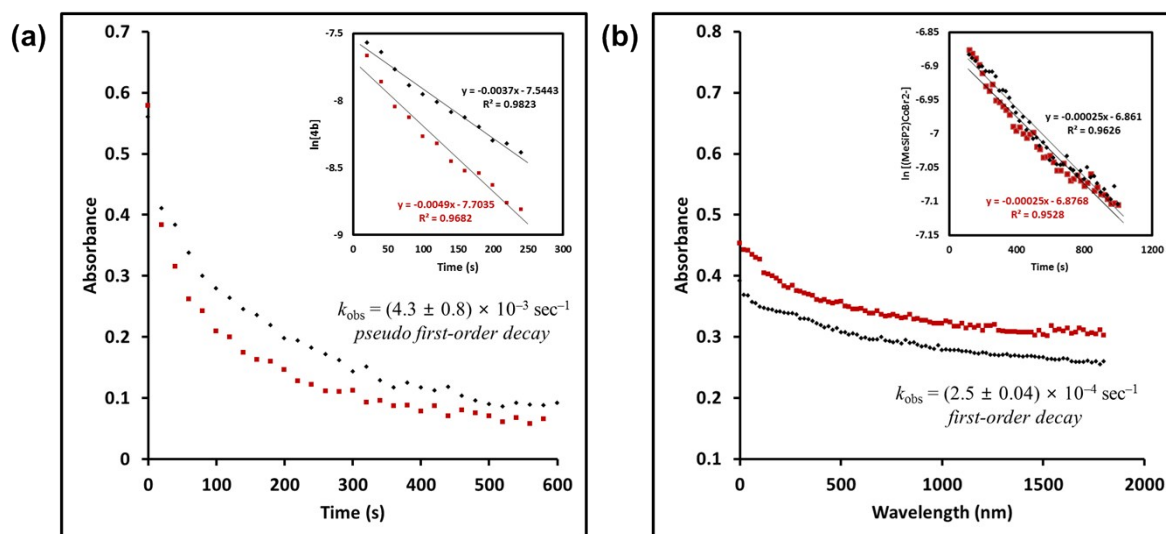


**Figure S38.** Plots of absorbance vs. time monitored (a) at  $\lambda_{\text{max}} = 450\text{ nm}$  for the reaction of **3b** with 100 equiv. of triethylamine at  $-40\text{ }^{\circ}\text{C}$ , (Inset) a plot of  $\ln[\mathbf{3b}]$  vs. time with a linear least-square fit and (b) at  $\lambda_{\text{max}} = 688\text{ nm}$  after the temperature increased to  $20\text{ }^{\circ}\text{C}$ , (Inset) a plot of  $\ln[(\text{MeSiP}_2)\text{CoBr}_2^-]$  vs. time with a linear least-square fit.



*Determination of thermal expansion coefficient of tetrahydrofuran.* We determined the average volumetric thermal expansion coefficient of THF ( $\alpha_V^{\text{THF}}$ ) at 20 °C - -35 °C. A 20 mL volumetric flask was filled with 20 mL of THF at room temperature and cooled down to -35 °C. The contracted volume of THF was measured as 18.8 mL, by comparing the same volume of the water at 20 °C. To compensate the thermal contraction of the volumetric flask, we measured the change of the height of the volumetric flask at 20 °C and -35 °C. The 20 mL volumetric flask is assumed to be a 5.00-cm height cone. At -35 °C, it was contracted to a 4.89-cm height cone. From this result, we estimated the 7% volumetric contraction of the 20 mL volumetric flask.

Thus, the modified volume of THF at -35 °C is

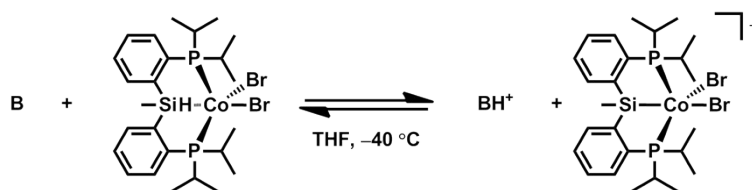
$$18.8 \text{ mL} \times 0.93 = 17.5 \text{ mL}$$

$\alpha_V^{\text{THF}}$  has been calculated as follows:

$$\alpha_V^{\text{THF}} = \frac{\Delta V}{V\Delta T}$$

V is the initial volume of THF at 25 °C (20 mL),  $\Delta V$  is the change of the volume of THF (-2.5 mL), and  $\Delta T$  is the change in temperature (-55 °C). From this calculation, the  $\alpha_V^{\text{THF}}$  is estimated to be 0.0023.

***pK<sub>a</sub> measurement for (MeSi<sup>H</sup>P<sub>2</sub>)CoBr<sub>2</sub> (3b).***



*Solution A* was prepared by dissolving cobalt(II) bromide (48.1 mg, 220  $\mu\text{mol}$ ) in 20 mL THF at 20 °C (11.0 mM). *Solution B* was prepared by dissolving MeSi<sup>H</sup>P<sub>2</sub> (43.0 mg, 99.9  $\mu\text{mol}$ ) in 10 mL THF at 20 °C (9.99 mM). *Solution C* was prepared by dissolving base (500  $\mu\text{mol}$ ) in 5.0 mL of THF at 20 °C. *Solution A* (1.0 mL) was added to a certain amount of THF ( $V_{\text{THF}}$ ) and cooled to -40 °C. To the solution was added *Solution B* (1.0 mL) in 1 mL of THF at -40 °C, resulting in a pale green solution. After 5 minutes, *Solution C* was added to the resulting solution of **3b**. The solution was monitored by UV-Vis spectroscopy at -40 °C. The absorbance at 450 nm was measured to determine the concentration of **3b** at equilibrium state.

The  $pK_a$  value of **3b** was estimated as follows:

$$V_i = V_{RT}(1 - \alpha_V^{\text{THF}}\Delta T), V_f = V'_{RT}(1 - \alpha_V^{\text{THF}}\Delta T), C^{\text{Complex}} = \frac{n^{\text{Complex}}}{V_i}, C^{\text{Base}} = \frac{n^{\text{Base}}}{V_f}$$

(where  $V_i$  = volume of the solution of **3b** at -40 °C,  $V_f$  = volume of the solution after the addition of the base at -40 °C,  $V_{RT}$  = total volume of the solution of **3b** at 20 °C,  $V'_{RT}$  = total volume of the solution of **3b** and *Solution C* at 20 °C,  $C^{\text{Complex}}$  = initial molar concentration of **3b** at -40 °C before the addition of the base,  $C^{\text{Base}}$  = initial molar concentration of the base at -40 °C after addition,  $n^{\text{Complex}}$  = mole of **3b**, and  $n^{\text{Base}}$  = mole of the base)

$$[(MeSi^H P_2)CoBr_2] = \frac{A_f V_i}{A_i V_f} C^{Complex}, [B] = C^{Base} - [BH^+]$$

(where  $A_i$  = initial absorbance of **3b** in the solution, and  $A_f$  = final absorbance of **3b** in the solution at equilibrium state)

$$[BH^+] = [(MeSiP_2)CoBr_2^-] = C^{Complex} - [(MeSi^H P_2)CoBr_2]$$

$$K = \frac{[BH^+][ (MeSiP_2)CoBr_2^- ]}{[B][ (MeSi^H P_2)CoBr_2 ]} = \frac{K_a^{Complex}}{K_a^{Base}}$$

$$pK_a^{Complex} = -\log_{10}(KK_a^{Base})$$

**Table S9.**  $pK_a$  value of **3b** ( $pK_a^{Complex}$ ).

Base	Pyrrolidine	Triethylamine	Proton sponge
$V_{THF}$ (mL)	8.0	8.0	11
<i>Solution C</i> (mL)	0.10	1.0	1.0
$pK_a^{Base}$	13.5	12.5	11.1
$K$	3.92	$6.49 \times 10^{-1}$	$3.92 \times 10^{-2}$
$pK_a^{Complex}$	12.9	12.7	12.5

**Figure S39.** UV-Vis spectra of **3b** (blue line in each spectrum) and the mixture of **3b** and a deprotonated intermediate in equilibrium after addition of base (~10 equiv., top: pyrrolidine, middle: triethylamine, bottom: proton sponge) in THF, measured at  $-40\text{ }^{\circ}\text{C}$ .

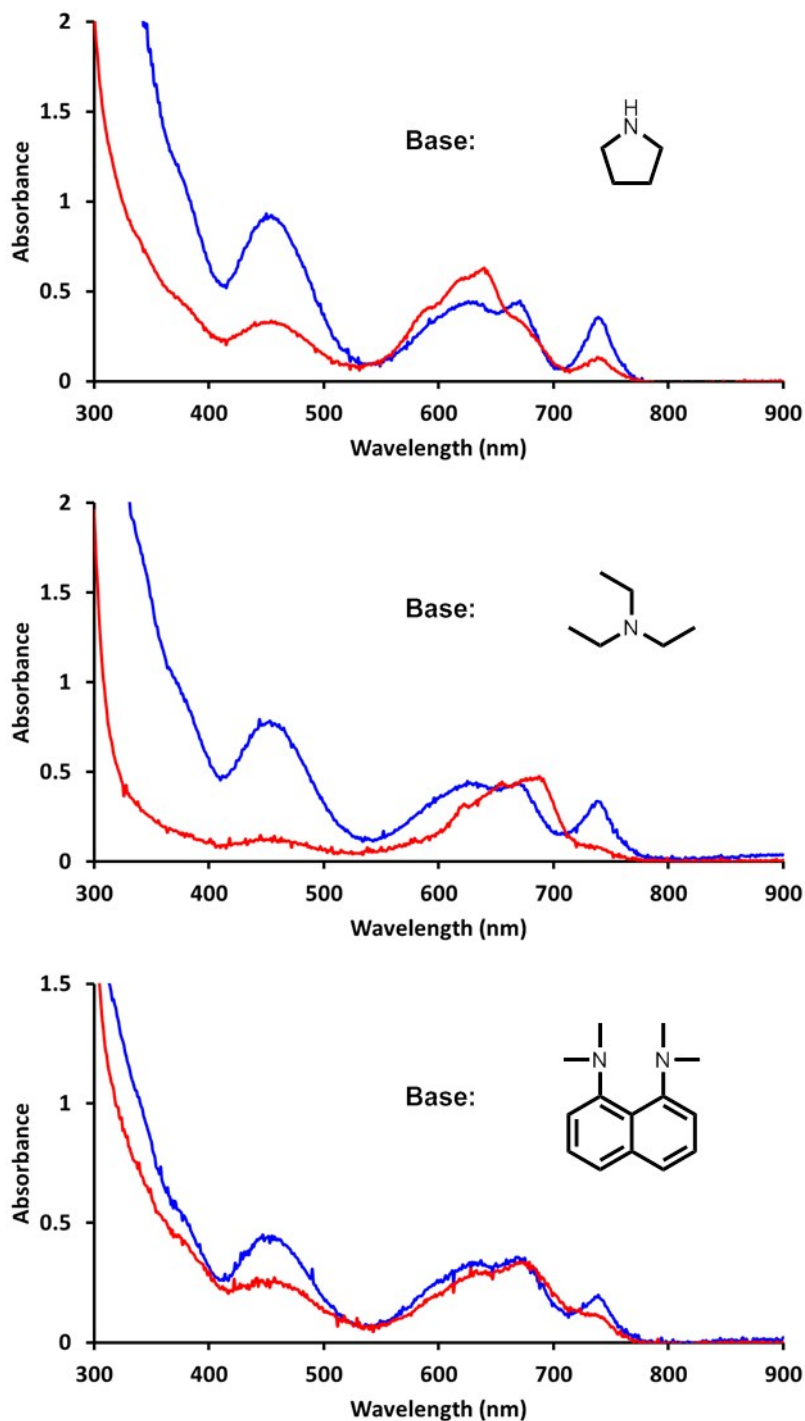


Figure S40. IR spectrum of **a** at room temperature. (KBr pellet)

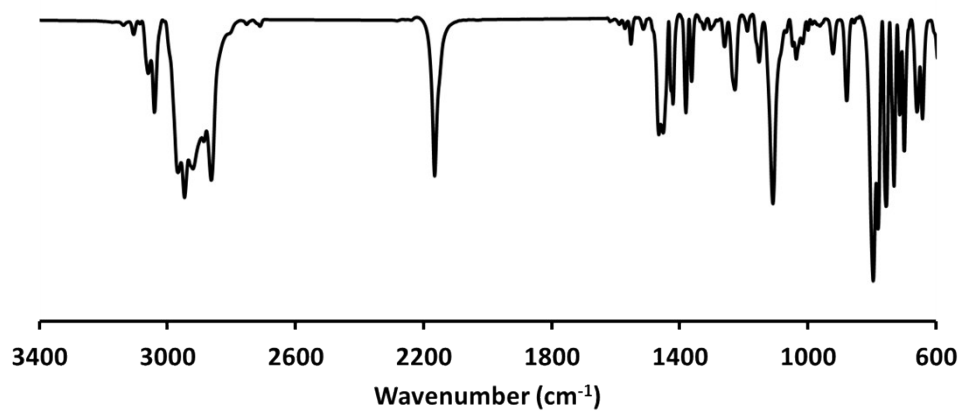


Figure S41. IR spectra of **b-D** (red line) and **b** (blue line) at room temperature. (KBr pellet)

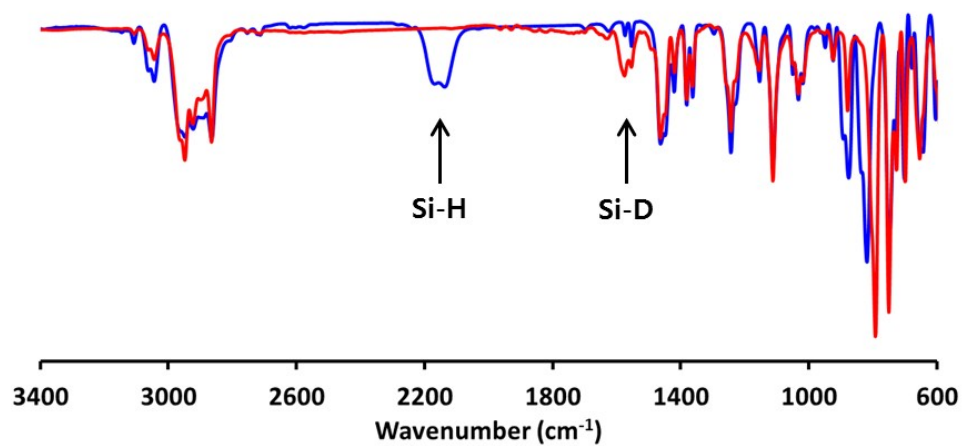
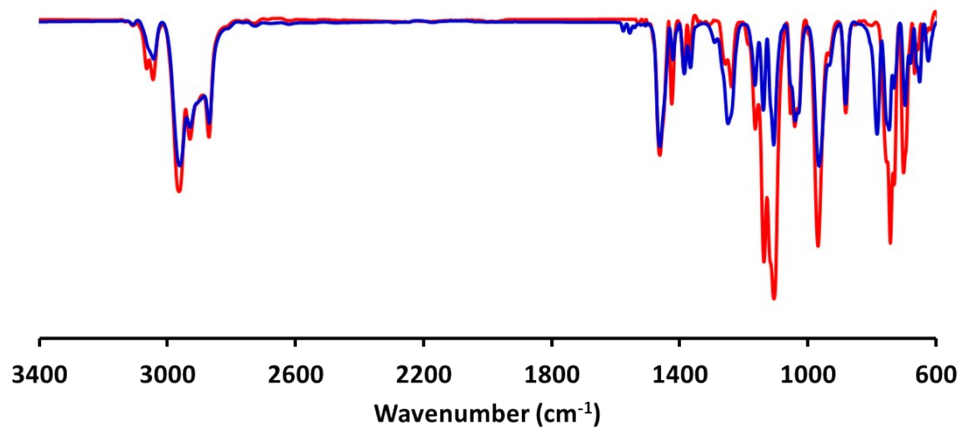
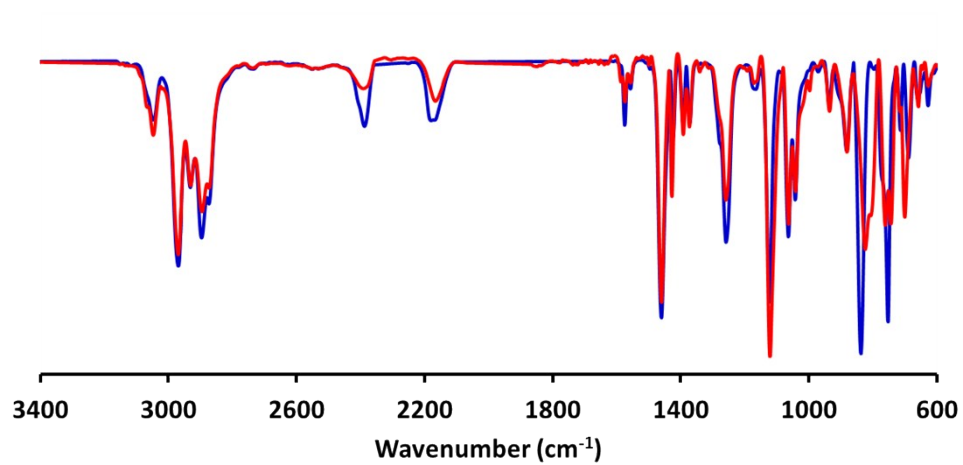


Figure S42. IR spectra of **1a** (red line) and **1b** (blue line) at room temperature. (KBr pellet)



**Figure S43.** IR spectra of **2a** (red line) and **2b** (blue line) at room temperature. (KBr pellet)



**Figure S44.** IR spectra of **3b-D** (red line) and **3b** (blue line) at room temperature. (KBr pellet)

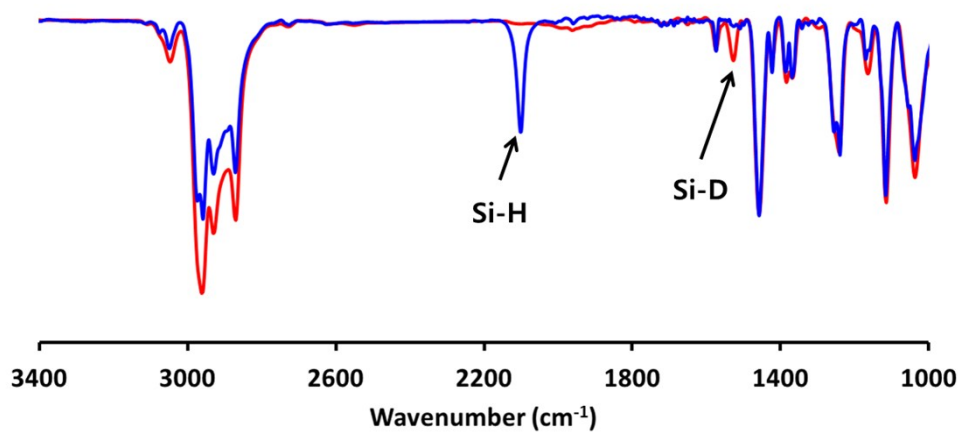


**Figure S45.** ESI mass data of **a**; blue bars represent calculated values and red bars represent experiment values.

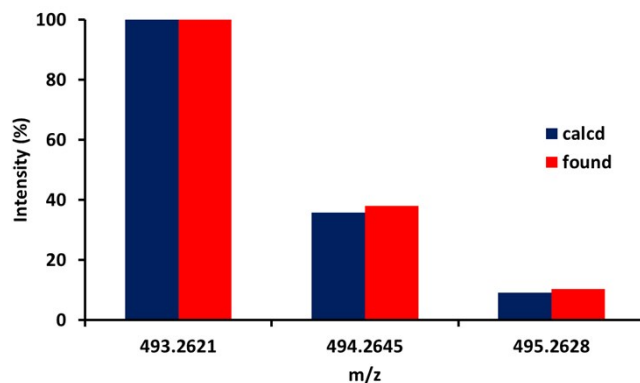


**Figure S46.** ESI mass data of **MeSiP<sub>2</sub>Cl**; blue bars represent calculated values and red bars represent experiment values.

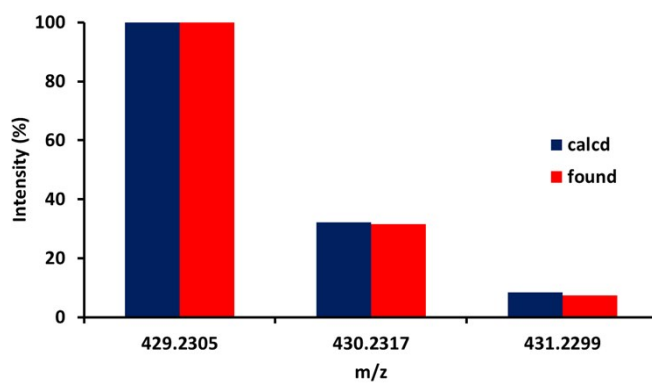
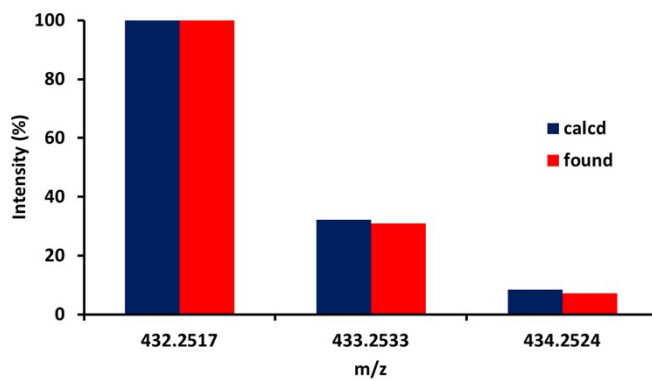


**Figure S47.** ESI mass data of **b-D**; blue bars represent calculated values and red bars represent experiment values.



**Computational Details.** All geometry optimizations and frequency calculations were carried out using DFT as implemented in the Jaguar 8.9 suite of ab initio quantum chemistry programs.<sup>9</sup> Geometry optimizations were performed with M06 functional<sup>10</sup> and the 6-31G\*\* basis set.<sup>11</sup> Cobalt was represented using the Los Alamos LACVP basis<sup>11</sup> that includes effective core potentials. The energies of the optimized structures were re-evaluated by additional single-point calculations on each optimized geometry using Dunning's correlation consistent triple- $\zeta$  basis set ccpVTZ(-f) that includes a double set of polarization functions. For Co, a modified version of LACVP, designated LACV3P, in which the exponents were decontracted to match the effective core potential with triple- $\zeta$  quality. Analytical vibrational frequencies within the harmonic approximation were computed with the 6-31G\*\*/LACVP basis to confirm proper convergence to well-defined minima on the potential energy surface. Solvation energies were evaluated by a self-consistent reaction field (SCRF) approach based on accurate numerical solutions of the Poisson–Boltzmann equation.<sup>12</sup> In the results reported, solvation calculations were carried out with the 6-31G\*\*/LACVP basis at the optimized gas-phase geometry employing the dielectric constant of  $\epsilon = 7.52$  for THF. As is the case for all continuum models, the solvation energies are subject to empirical parametrization of the atomic radii that are used to generate the solute surface. We employed the standard set of optimized radii in Jaguar for H (1.150 Å), C (1.900 Å), N (1.600 Å), and Co (1.436 Å).<sup>13</sup> To compute  $pK_a$ , the free energy in solution-phase G(sol) has been calculated as follows:

$$G(\text{sol}) = G(\text{gas}) + \Delta G^{\text{solv}}$$

$$G(\text{gas}) = H(\text{gas}) - TS(\text{gas})$$

$$H(\text{gas}) = E(\text{SCF}) + \text{ZPE}$$

$$\Delta E(\text{SCF}) = \Sigma E(\text{SCF}) \text{ for products} - \Sigma E(\text{SCF}) \text{ for reactants}$$

$$\Delta G(\text{sol}) = \Sigma G(\text{sol}) \text{ for products} - \Sigma G(\text{sol}) \text{ for reactants}$$

$G(\text{gas})$  is the free energy in the gas phase;  $G(\text{sol})$  is the free energy of solvation as computed using the continuum solvation model;  $H(\text{gas})$  is the enthalpy in gas phase;  $T$  is the temperature (298.15K);  $S(\text{gas})$  is the entropy in the gas phase;  $E(\text{SCF})$  is the self-consistent field energy, i.e., raw electronic energy as computed from the SCF procedure; and ZPE is the zero-point energy. Note that by entropy here we refer specifically to the vibrational/rotational/translational entropy of the solute(s); the entropy of the solvent is incorporated implicitly in the continuum solvation model. An NBO analysis (version 6.0) as implemented in Jaguar<sup>14</sup> was used to elucidate the bond order for the key atoms.

---

<sup>9</sup> Jaguar 7.0; Schrödinger, LLC: New York, 2007.

<sup>10</sup> Y. Zhao and D. G. Truhlar, *Theor. Chem. Acc.*, 2008, **120**, 215.

<sup>11</sup> (a) P. J. Hay and W. R. Wadt, *J. Chem. Phys.*, 1985, **82**, 270; (b) W. R. Wadt and P. J. Hay, *J. Chem. Phys.*, 1985, **82**, 284; (c) P. J. Hay and W. R. Wadt, *J. Chem. Phys.*, 1985, **82**, 299.

<sup>12</sup> (a) B. Marten, K. Kim, C. Cortis, R. A. Friesner, R. B. Murphy, M. N. Ringnalda, D. Sitkoff and B. Honig, *J. Phys. Chem.*, 1996, **100**, 11775; (b) S. R. Edinger, C. Cortis, P. S. Shenkin and R. A. Friesner, *J. Phys. Chem. B*, 1997, **101**, 1190; (c) M. Friedrichs, R. Zhou, S. R. Edinger and R. A. Friesner, *J. Phys. Chem. B*, 1999, **103**, 3057.

<sup>13</sup> A. A. Rashin and B. Honig, *J. Phys. Chem.*, 1985, **89**, 5588.

<sup>14</sup> (a) A. E. Reed, L. A. Curtiss and F. Weinhold, *Chem. Rev.*, 1988, **88**, 899; (b) A. E. Reed, R. B. Weinstock and F. Weinhold, *J. Chem. Phys.*, 1985, **83**, 735.

*DFT calculation of  $pK_a$  value of **3b**.* Gibbs free energy of the intermediates (**INT1**, **INT3**) along with the solvation energy of  $H^+$  in THF was determined. We first calculated the solvation energy of protonated THF and then only THF. The difference in the solvation energies of protonated-THF and THF provided a value of  $-250.42$  kcal/mol. It was used as the solvation energy  $[G(\text{solv})_{\text{proton}}]$  of proton in THF.  $G(\text{sol})$  is the Gibbs free energy of a species in solution, obtained by summing the gas phase free energy  $[G(\text{gas})]$  and the solvation energy  $[G(\text{solv})]$  as computed using the continuum solvation model.

Thus,  $G(\text{sol}) = G(\text{gas}) + G(\text{solv})$  (Eqn 1)

Now,

$$\Delta G(\text{sol}) = [G(\text{sol})_{\text{INT3}} + G(\text{solv})_{\text{proton}} - G(\text{sol})_{\text{INT1}}] \times 23.0605423 \text{ kcal/mol} \text{ (Eqn 2)}$$

( $\Delta G(\text{sol})$  is the change in free energy in solution during deprotonation)

Again,  $pK_a = \Delta G(\text{sol}) / (2.303RT)$  (Eqn 3) (where  $R$  = universal gas constant,  $T$  = temperature)

The Gibbs free energies in solution of **INT1** ( $-57676.268$  eV), **INT3** ( $-57664.292$  eV) and proton ( $-11.196$  eV) were set into Eqn 2 to determine change in the free energy  $[\Delta G(\text{sol})]$  during deprotonation of **INT1**. Now the value  $\Delta G(\text{sol})$  obtained from Eqn 2 substituted to Eqn 3 to obtain the  $pK_a$ . Calculation showed the value to be 13.23.

*Details of computations for reaction pathway 1.* Hydrosilylation normally proceeds via oxidative addition followed by reductive elimination (Scheme 4, pathway 1). According to the pathway 1, the Co(II) ion in **3b** (**INT1**) oxidizes to Co(IV) in **INT2** by oxidative addition. This must lead to a change of geometry from distorted trigonal bipyramidal (TBP) to octahedral coordination at the cobalt centre. Following reductive elimination of HBr from **INT2** forms a distorted square planar product **1b** (**INT4**). We tried to compute this mechanistic pathway assuming both high spin and low spin Co(IV). We were unable to locate a Co(IV)-hydrido complex corresponding to **INT2**. At first we generated an ideal input structure (**INT2\***) locating the coordinates of Si, Co and H assuming the oxidative addition product. Here the Si-Co distance was kept at  $2.25 \text{ \AA}$  (in accordance with the optimized structure of **INT4**) and Si-Co-H angle was kept at  $90^\circ$  in the input file (keeping in mind that, oxidative addition will generate an octahedral structure). We computed the structure using the above-mentioned conditions and took out the optimized coordinates as an input structure for the oxidative addition product assuming low spin Co(IV). Enforcing no geometrical constraints in the input file we surprisingly found that the hydrogen flips back to the Si centre forming previously mentioned  $\eta^1$ -type (2-center-2-electron) [Si-H]-Co bond and we could only locate this result (**INT2-LS**) lower in energy by  $29.66$  kcal/mol than the input structure. This energy minimized structure is slightly different from **INT1**. The aromatic rings of **INT2-LS** are slightly flanked outwards and the energy of **INT2-LS** is  $4.62$  kcal/mol lower than that of **INT1**. This is expected since the solid state structure will only prefer a more closely packed geometry of the compound. Similar calculations were performed assuming the high spin Co(IV)-hydrido complex. But we could not locate a reasonable structure. The optimized geometry (**INT2-HS**) was distorted and  $73.43$  kcal/mol higher in energy relative to that of **INT1**.

**Figure S48.** Plausible mechanisms of **1b** (**INT4**) formation from intermediate **3b** (**INT1**).

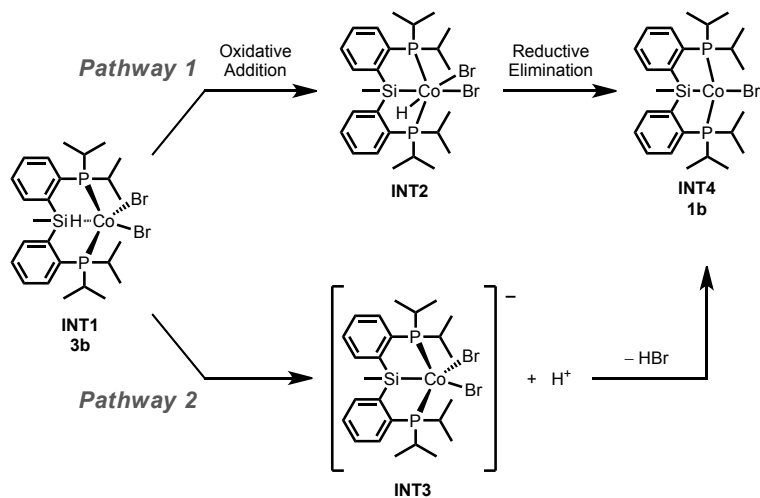


**Figure S49.** A relative free energy (kcal/mol) profile for pathway 2 involving deprotonation and dehalogenation from **INT1**. Calculation was conducted in a THF solution. Hydrogen atoms except Si–H are omitted for clarity.

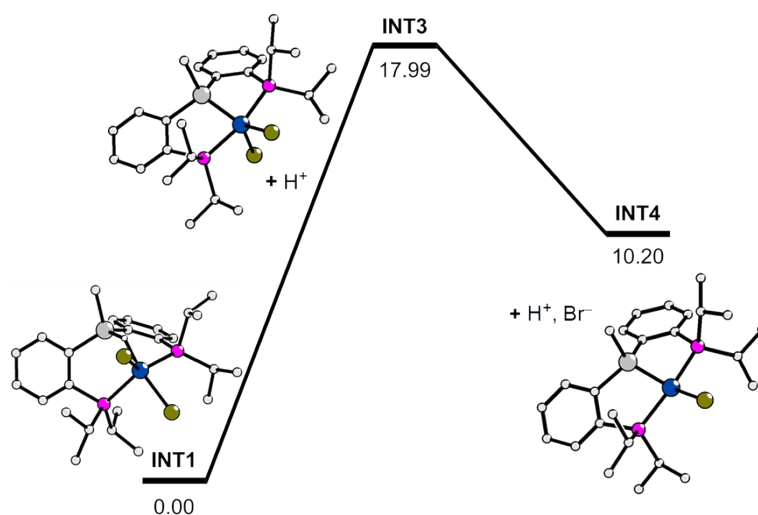


**Table S10.** Selected bond indices for **1b** and **3b** from NBO analysis.

	<b>1b</b>		<b>3b</b>	
	Mayer-Mülliken	Wiberg	Mayer-Mülliken	Wiberg
Si–H	-	-	0.501	0.618
Co–H	-	-	0.443	0.193
Co–Si	0.830	0.551	0.313	0.122

**Table S11.** Cartesian coordinates (Å) for the optimized structure of INT1.

Co1	2.7759133558	4.8933617867	3.8535425152
P2	2.6058553158	5.1558770926	6.1494931201
P3	1.6897937583	2.9770115101	2.9117145861
Si4	4.5018026478	2.9494555849	4.5670738455
Br5	0.9050558194	6.3274456334	3.3649997182
Br6	4.2385147666	5.9647617426	2.1244844658
C7	2.9029516456	3.5225495955	6.9449321217
C8	4.1530295274	6.0861123303	6.6646147112
C9	1.2116570965	5.9055649225	7.1366435145
C10	2.7829392042	1.4972210130	2.7894630044
C11	1.3042605486	3.3844665650	1.1148901000
C12	0.1374671516	2.1980621519	3.6109984026
C13	6.3650581795	3.0966970608	4.7070234722
C14	3.7240323111	2.6151384087	6.2481187501
C15	4.0518264415	1.5690707585	3.3851226890
H16	4.2562729015	4.3906996790	4.0853124104
H17	0.9633695382	7.6476064570	5.8497525324
H18	4.3338263302	7.1759026195	4.7739579609
H19	3.4125790171	3.8139097077	0.6991426875
C20	2.3484819576	3.1439433539	8.1702967755
C21	4.2575753615	6.3158871692	8.1659346395
H22	4.9465614935	5.3773012180	6.3740510837
C23	4.3559939059	7.3632280615	5.8551057101
C24	1.0638999330	7.4086031625	6.9148515994
H25	1.4883016336	5.7431135056	8.1903319871
C26	-0.1047663880	5.1954365914	6.8450118922
C27	2.4150791940	0.3422134629	2.0923818631
C28	2.5632875557	3.2803623399	0.2588736392
H29	1.0166721610	4.4447532448	1.1802749004
C30	0.1664100477	2.6014206508	0.4700974550
C31	-1.0118252437	3.1891674261	3.7267496429
H32	-0.1430272240	1.4057623221	2.8983685113
C33	0.4351837403	1.5505523063	4.9595851365
H34	6.8081040286	2.2143045350	5.1851423150
H35	6.6415772423	3.9725022867	5.3046706844
H36	6.8064452468	3.2176519500	3.7109339366
C37	3.9744517874	1.3600799614	6.8128283597
C38	4.9395608191	0.4965100123	3.2255725655
H39	1.7045295572	3.8274997127	8.7203315658
C40	2.5940467019	1.8834119881	8.7049047374
H41	5.2453794694	6.7260991549	8.4107171144
H42	4.1307627309	5.3888534142	8.7386371806
H43	3.5138303335	7.0413522155	8.5183992458
H44	3.5916261912	8.1160218791	6.0769998250
H45	5.3314941892	7.8018559348	6.1005346230
H46	1.9050624801	7.9784418003	7.3226320185
H47	0.1560889208	7.7567450442	7.4241889456
H48	-0.8733964223	5.5319377948	7.5522885933
H49	-0.0344239118	4.1027807855	6.9217873053
H50	-0.4417169518	5.4511191814	5.8334395316
H51	1.4270372390	0.2673758288	1.6414111454
C52	3.3022549776	-0.7189545638	1.9525535563
H53	2.8483040402	2.2326449038	0.0968978155
H54	2.3700330068	3.7297995067	-0.7230777862
H55	-0.0187408298	3.0108765982	-0.5312139761
H56	-0.7772194607	2.6570130695	1.0222113870
H57	0.4224393349	1.5429046724	0.3319229540
H58	-1.9136923453	2.6719411968	4.0799452366
H59	-1.2520360851	3.6855326440	2.7801389889
H60	-0.7701829712	3.9812338172	4.4422978036
H61	0.8065349872	2.2887950547	5.6842588794
H62	1.1860680161	0.7546101819	4.8863888615
H63	-0.4815163420	1.1113145152	5.3742830384
C64	3.4108204543	0.9873672894	8.0276955480
H65	4.5999245219	0.6416027864	6.2787889084
C66	4.5736893749	-0.6370591394	2.5100558613
H67	5.9359200267	0.5434976224	3.6664198578
H68	2.1423373321	1.6032413922	9.6540125833
H69	3.0029358749	-1.6064665993	1.3995424527
H70	3.6015604064	-0.0011785534	8.4392496864
H71	5.2779470619	-1.4574820501	2.3910823057

**Table S12.** Cartesian coordinates (Å) for the initial structure of INT2 (INT2\*).

Co	2.9228244120	4.4801281570	4.0510651470
P	3.5253831990	5.6280259630	5.9702185600
P	2.8806758190	2.9321789160	2.3219723840
Si	4.8704671160	3.4474890370	4.5014415040
Br	1.7417012230	2.8046365160	5.5693325760
Br	1.1230485320	5.7770427470	2.9896150110
C	4.5848656120	4.5592392990	7.0209798240
C	4.4944814590	7.1610231920	5.5181332610
C	2.0746436080	6.0542672320	7.0963218430
C	4.0900793360	1.5770558630	2.5654465680
C	3.2938047250	3.6838091800	0.6619176970
C	1.1302488790	2.2370767710	2.1918242970
C	6.4347439470	4.3509177120	3.9141738380
C	5.0995874100	3.4273749700	6.3697339590
C	4.9674863000	1.7707492780	3.6414939330
H	3.5715287710	5.3639532270	3.2722190900
H	2.3427381950	8.1719160390	7.5498060930
H	2.9755310120	7.7864367780	4.0729590980
H	4.5744237560	5.2542694450	1.4717811310
C	4.7974982460	4.7378202920	8.3892197040
C	5.3810560140	7.7357211090	6.6144498360
H	5.1456474530	6.7677666330	4.7233129480
C	3.5884857630	8.2089938080	4.8787262480
C	2.3404065870	7.2049673790	8.0660552190
H	1.9869697570	5.1122438650	7.6573750970
C	0.7536171200	6.2904503290	6.3791169460
C	4.2164477790	0.4459314170	1.7492892810
C	4.6011857720	4.4602053320	0.7178289940
H	2.4710792970	4.3962241950	0.5060884260
C	3.3409119610	2.6847405000	-0.4895864930
C	1.0635782700	0.7157612380	2.1308447390
H	0.7148287330	2.5433601590	3.1602324920
C	0.2888222250	2.8606769470	1.0848104030
H	7.2990725480	3.6962032480	4.0958759820
H	6.6091317410	5.2771021820	4.4758275330
H	6.4119660740	4.5923741340	2.8465108200
C	5.8123847430	2.4850645370	7.1098820820
C	5.9699798020	0.8217536010	3.8738049890
H	4.3944217220	5.6006636590	8.9130947020
C	5.5143439160	3.7899172930	9.1115897140
H	6.0160861190	8.5250242170	6.1925700810
H	6.0387360340	6.9749811420	7.0509956730
H	4.7971194610	8.1885872570	7.4235644410
H	2.9146347290	8.6676547550	5.6122458240
H	4.2014610430	9.0133317870	4.4537389390
H	3.2738725340	7.1255096380	8.6300365980
H	1.5215417230	7.2364510300	8.7951719460
H	-0.0299961150	6.4288618280	7.1347423010
H	0.4762038540	5.4439498270	5.7475800280
H	0.7786500350	7.1907147730	5.7541150840
H	3.5418760200	0.2865742810	0.9122705320
C	5.2055977970	-0.4944093670	2.0085993340
H	5.4441753370	3.7915642490	0.9413743080
H	4.8003727770	4.9244141690	-0.2555780580
H	3.4002466410	3.2291865280	-1.4405062680
H	2.4662827980	2.0283846260	-0.5418222240
H	4.2352934050	2.0542417840	-0.4198576620
H	0.0166361340	0.4133535220	2.2542496680
H	1.6408386420	0.2360165940	2.9273903420
H	1.3976076870	0.3205215310	1.1627546160
H	0.6219683670	2.5685169520	0.0822053360
H	0.2579996520	3.9519345460	1.1454943630
H	-0.7410798750	2.5007486830	1.1980095480
C	6.0153161530	2.6609366870	8.4745962870
H	6.1934790630	1.5861668910	6.6272223020
C	6.0827589130	-0.3088434870	3.0741266920
H	6.6862442940	0.9710191540	4.6820151750
H	5.6681823140	3.9295265290	10.1792098230
H	5.2941293430	-1.3726460200	1.3734622620
H	6.5581112000	1.9104090130	9.0452657440
H	6.8614361760	-1.0418786030	3.2730438800

**Table S13.** Cartesian coordinates (Å) for the optimized structure of INT2-LS.

Co1	2.7891960833	4.3715973078	4.1047955940
P2	3.1851684163	5.5951113046	5.9721163704
P3	2.6299613858	2.8915631644	2.4096827635
Si4	5.2920276983	3.6055371794	4.3365116063
Br5	1.9705009366	2.5721894317	5.5889195749
Br6	1.9634208583	6.2108054776	2.6822597295
C7	4.3588799537	4.5456806059	6.9295344889
C8	4.1633752616	7.1770599277	5.6999520478
C9	1.7095838883	5.8788844700	7.0787001034
C10	3.8702468453	1.5712038294	2.7685673805
C11	3.1243941467	3.4570826197	0.6988016726
C12	0.8605950127	2.2647542329	2.2899149312
C13	6.9855949863	4.2037568117	3.7746029539
C14	5.2593726568	3.7294618509	6.2147764426
C15	4.9785377780	1.9033498406	3.5811818527
H16	4.4066663678	4.6826379020	3.6848478882
H17	1.8097303908	7.9439954831	7.7730500490
H18	2.5888320725	8.1194056161	4.5085156480
H19	4.5288279980	4.9627214105	1.4074876877
C20	4.3692751268	4.5210619846	8.3244861487
C21	5.1163971917	7.5393421780	6.8341465890
H22	4.7622282765	6.9089831349	4.8132358403
C23	3.2864374342	8.3644342044	5.3153277293
C24	1.8329189674	6.9276675091	8.1813533871
H25	1.5935168190	4.8834600941	7.5348607259
C26	0.4721808751	6.1449047928	6.2239455820
C27	3.8030046091	0.2976739003	2.1948801630
C28	4.5018278910	4.1052897823	0.7252377764
H29	2.3864373815	4.2374205975	0.4663677786
C30	3.0706617748	2.3569769606	-0.3549877716
C31	0.6212601823	0.7803370076	2.0545620600
H32	0.5065460615	2.4878129266	3.3048956676
C33	0.0553952081	3.1261248696	1.3205820291
H34	7.7877702204	3.5723575440	4.1757692681
H35	7.1594555941	5.2244710750	4.1370731801
H36	7.0715775123	4.2066592086	2.6822914559
C37	6.1675802135	2.9473502217	6.9353675736
C38	5.9645940161	0.9321667249	3.7898965859
H39	3.6634969086	5.1244357327	8.8898039109
C40	5.2640556359	3.7149605792	9.0202659388
H41	5.6826366023	8.4388651828	6.5587841301
H42	5.8352756049	6.7421253384	7.0528227941
H43	4.5750113259	7.7685612259	7.7611816963
H44	2.7196611043	8.7403554730	6.1748646433
H45	3.8248316465	9.1870579722	4.9689958646
H46	2.7392823267	6.8380501498	8.7893848173
H47	0.9733846372	6.8372688387	8.8579640804
H48	-0.4139354002	6.2007833356	6.8693519316
H49	0.3128298703	5.3500550898	5.4872980659
H50	0.5511625164	7.0919856196	5.6761432047
H51	2.9739386054	0.0368424108	1.5442571545
C52	4.7835264847	-0.6587916775	2.4395891377
H53	5.2755974425	3.3814398789	1.0199866577
H54	4.7613929764	4.4673507467	-0.2775536074
H55	3.2754733714	2.7839200484	-1.3453384847
H56	2.0957011735	1.8583408806	-0.4073086701
H57	3.8336756167	1.5909097536	-0.1659598325
H58	-0.4561145727	0.5847782750	2.1333881280
H59	1.1218835190	0.1579977873	2.8035566107
H60	0.9307169550	0.4542805498	1.0523106078
H61	0.3164351345	2.9300647027	0.2729290063
H62	0.1798294845	4.1974291546	1.5175215118
H63	-1.0087935901	2.8863951482	1.4385201339
C64	6.1738774630	2.9306410281	8.3255562193
H65	6.8795311192	2.3141481880	6.4033688043
C66	5.8681112990	-0.3430910431	3.2448204182
H67	6.8400331768	1.1718473068	4.3956239537
H68	5.2463375841	3.7027172289	10.1078008010
H69	4.6980250356	-1.6463121380	1.9920721846
H70	6.8788432628	2.2992374309	8.8616859303
H71	6.6427799081	-1.0810647628	3.4408833206

**Table S14.** Cartesian coordinates (Å) for the optimized structure of INT2-HS.

Co	2.2945063084	4.6275714302	4.0258579610
P	3.4555678901	5.6108586307	6.0462577075
P	2.9378510374	2.9142914732	2.3237793425
Si	5.6201087303	3.7021298111	4.3587071156
Br	1.7688802556	2.7294491479	5.5948092906
Br	0.3735258998	5.6507086529	3.0623473716
C	4.5668490432	4.4634719874	6.9630565228
C	4.5698148215	7.0096044521	5.4959718243
C	2.2251877855	6.2167237685	7.3203915137
C	4.2694071968	1.6842021399	2.6934464735
C	3.4983012556	3.6181445782	0.6817866514
C	1.2492457074	2.0857037248	2.0780325844
C	7.3387896593	4.3375799453	3.9036685572
C	5.4818389289	3.6668597111	6.2426784542
C	5.3507569252	2.0144185276	3.5420847403
H	3.4465023815	5.6206957405	3.3131226039
H	2.8622281876	8.2386716738	7.8207250941
H	3.0117620573	7.8163379869	4.2014822680
H	4.6340415488	5.2205734634	1.6420418209
C	4.4982042686	4.3406568033	8.3538739465
C	5.6225290717	7.4662112027	6.4961763414
H	5.0814286096	6.5416733488	4.6362120578
C	3.7418712670	8.1641703424	4.9432467473
C	2.7266037077	7.2660506802	8.3094606664
H	1.9908583310	5.2851233637	7.8587384773
C	0.9348764990	6.6809094498	6.6504117054
C	4.2739153103	0.4461326251	2.0368015215
C	4.7638367961	4.4473758431	0.8733948771
H	2.6768788199	4.2948889242	0.4020452573
C	3.7139189317	2.5805930518	-0.4138864576
C	1.1480696762	0.5678149124	2.1439908634
H	0.7411326924	2.4613843322	2.9773896158
C	0.4936686754	2.6356821362	0.8729495851
H	8.1288009377	3.7136536030	4.3448184341
H	7.4770355821	5.3564066690	4.2855500042
H	7.4871286256	4.3560821622	2.8183938006
C	6.3234817824	2.8068805575	6.9576932266
C	6.3750839121	1.0701098313	3.7041469875
H	3.7808399318	4.9213847309	8.9269173514
C	5.3338224463	3.4659703068	9.0386387110
H	6.3060333668	8.1757923188	6.0109401812
H	6.2209786817	6.6299435469	6.8766091795
H	5.1777484943	7.9807600366	7.3555646442
H	3.2060822666	8.6989997156	5.7377671707
H	4.3998904986	8.8909994038	4.4506383075
H	3.6742094716	7.0012156999	8.7911494903
H	1.9783262165	7.4083020876	9.1003600124
H	0.2046579539	6.9659960936	7.4186966746
H	0.4874535206	5.8907459227	6.0382949620
H	1.0948725476	7.5537378710	6.0052052827
H	3.4763150535	0.1971907939	1.3448812148
C	5.2924926840	-0.4789168433	2.2315834668
H	5.6086092198	3.8033031462	1.1583788350
H	5.0334387906	4.9392519529	-0.0699636176
H	3.9328852892	3.0855627376	-1.3636604692
H	2.8457777863	1.9320512596	-0.5757303683
H	4.5729631571	1.9396998667	-0.1784576388
H	0.0929599471	0.3025624639	2.2885418252
H	1.7095037966	0.1425501937	2.9819975129
H	1.4710337379	0.0844872803	1.2124407222
H	0.8882323555	2.2576826836	-0.0778828251
H	0.4843771344	3.7306754856	0.8430869198
H	-0.5527974423	2.3123434039	0.9415758658
C	6.2575789641	2.6998564195	8.3417882356
H	7.0413468597	2.1855402623	6.4199914509
C	6.3479999791	-0.1691676468	3.0776734400
H	7.2327795831	1.3115307708	4.3338553971
H	5.2585045524	3.3871055078	10.1209003978
H	5.2617293800	-1.4330694282	1.7106806095
H	6.9172411790	2.0153850030	8.8706216279
H	7.1558376076	-0.8801933569	3.2369355558

**Table S15.** Cartesian coordinates (Å) for the optimized structure of **INT3**.

Co1	2.6410275319	3.9539044789	4.4048063358
P2	3.2558041323	5.1566615546	6.1863474317
P3	2.4890686434	2.4275130576	2.7630879709
Si4	4.7347640824	3.1513314538	4.6386640439
Br5	1.3391444226	2.3857770622	6.1210801491
Br6	1.4647562692	5.8153818406	3.0500038537
C7	4.3308785526	4.0748796728	7.2377938512
C8	4.3617901890	6.6384189377	5.8030033861
C9	1.8865565814	5.7082634044	7.3555521948
C10	3.7803515929	1.1105941734	2.9320400089
C11	2.7836299703	3.1045208630	1.0422258899
C12	0.8011351409	1.5994688429	2.7192268647
C13	6.3300653256	3.9722163025	3.9653596114
C14	5.0505134467	3.1036802003	6.5169785625
C15	4.8129251182	1.4176134283	3.8379378746
H16	2.2903049503	7.7846897366	7.8976863010
H17	2.8779652770	7.5703517731	4.5011768162
H18	4.2340513908	4.5419911188	1.7792212533
C19	4.4305084918	4.1275280150	8.6290941001
C20	5.3668254137	7.0237531486	6.8816384472
H21	4.9233791005	6.2516380843	4.9378957570
C22	3.5756349533	7.8453361215	5.3016409862
C23	2.2077847140	6.8005856730	8.3742168190
H24	1.6884581555	4.7640660601	7.8857682142
C25	0.6206744504	6.0704941483	6.5870675433
C26	3.8437703966	-0.0708707812	2.1799430285
C27	4.1468455104	3.7805405592	0.9946377348
H28	2.0195885498	3.8934339143	0.9730981458
C29	2.6283027943	2.1253949087	-0.1120033910
C30	0.6499989626	0.2065993496	2.1213024159
C31	0.6008359499	1.5177856174	3.7977354933
C32	-0.2263814882	2.5653872115	2.1382411292
H33	7.1941171613	3.3437544619	4.2279628471
H34	6.5046624570	4.9629816447	4.4051241503
H35	6.3094874964	4.0807687295	2.8745433215
C36	5.8745166744	2.2226035774	7.2200768658
C37	5.8754183715	0.5153091636	3.9711352701
H38	3.8541660190	4.8506736348	9.2018200689
C39	5.2435180508	3.2277317087	9.3118360172
H40	6.0361891484	7.8095799124	6.5021233989
H41	5.9866520906	6.1742146266	7.1918350732
H42	4.8721327226	7.4225045096	7.7766442627
H43	3.0061097102	8.3250151347	6.1071335305
H44	4.2720272805	8.5990517103	4.9071588649
H45	3.1307068982	6.6340316766	8.9400888407
H46	1.3849881678	6.8685224980	9.1004481981
H47	-0.1950471779	6.2634931517	7.2992064998
H48	0.3171237567	5.2582675929	5.9194766879
H49	0.7563888483	6.9688082689	5.9717108848
H50	3.0685011202	-0.3061240096	1.4552615787
C51	4.8965458852	-0.9641609813	2.3482187426
H52	4.9575105755	3.0471814964	1.1198552683
H53	4.2912547617	4.2735746230	0.0232544569
H54	2.8011399881	2.6439953420	-1.0661407727
H55	1.6281493183	1.6796065759	-0.1573216843
H56	3.3642257655	1.3116141750	-0.0487377248
H57	-0.3983823032	-0.1068337946	2.2296908846
H58	1.2644472193	-0.5353941562	2.6410621698
H59	0.8851858641	0.1642797441	1.0488113620
H60	-0.1121871385	2.6816117104	1.0507428538
H61	-0.1531525357	3.5608032933	2.5929607855
H62	-1.2376298092	2.1769894166	2.3218120544
C63	5.9711657165	2.2758790973	8.6072461024
H64	6.4306357239	1.4544968965	6.6802429433
C65	5.9140500533	-0.6733950716	3.2516998025
H66	6.7013988615	0.7500498665	4.6451937753
H67	5.2986004508	3.2653507202	10.3989586146
H68	4.9252735181	-1.8837267169	1.7654217328
H69	6.6021804222	1.5654236529	9.1403202155
H70	6.7439318741	-1.3670875597	3.3824235248

**Table S16.** Cartesian coordinates (Å) for the optimized structure of INT4.

Co1	2.8692606753	4.1369138261	4.2123783500
P2	3.2634153774	5.1642190387	6.1618021006
P3	2.5803548803	2.5191312929	2.7107326055
Si4	4.8139241786	3.0908829031	4.6567099751
Br5	1.7076831690	5.9181577814	2.9599138608
C6	4.2306207033	4.0052397439	7.2301129807
C7	4.3446016679	6.6894861261	5.9681559636
C8	1.7423300176	5.5001822492	7.2213381053
C9	3.7996944789	1.1470855886	2.8949196581
C10	2.6410840777	3.0387478669	0.9266683643
C11	0.8820415355	1.8074432787	3.0954097321
C12	6.3826785261	3.9795114108	4.0737625517
C13	4.9250216574	2.98711131632	6.5476707952
C14	4.8356750293	1.3928379133	3.8145232381
H15	1.7582664085	7.6072662380	7.7634809582
H16	2.8641584615	7.6947709723	4.7110473401
H17	4.2044250266	4.4897832474	1.3607710400
C18	4.2660191912	4.0612759264	8.6268260631
C19	5.2690433562	6.9888399472	7.1399311497
H20	4.9615507155	6.3831024584	5.1083366132
C21	3.5533439900	7.9183210284	5.5336283316
C22	1.8343897765	6.6269368908	8.2464280581
H23	1.6603275087	4.5458316334	7.7659199457
C24	0.4885975501	5.6602742516	6.3684370584
C25	3.7833713934	-0.0501894380	2.1663470516
C26	4.0113163937	3.6584629885	0.6717793297
H27	1.8927171504	3.8449492082	0.8923433959
C28	2.3131143088	1.9786071662	-0.1144437470
C29	0.6401345611	0.3426642265	2.7557765985
H30	0.8500951054	1.9074001000	4.1944473003
C31	-0.2143168813	2.6952179181	2.5143138871
H32	7.2537625375	3.3297752470	4.2373307801
H33	6.5525563491	4.9096991725	4.6292367950
H34	6.3325928269	4.2191677892	3.0054010885
C35	5.6363896795	2.0427462227	7.2944984609
C36	5.8372762230	0.4273610563	3.9756355812
H37	3.7293328679	4.8407561235	9.1653538945
C38	4.9721839918	3.1068810724	9.3495874894
H39	5.9274228064	7.8280681743	6.8797008843
H40	5.9022036814	6.1338638061	7.4034052720
H41	4.7090006773	7.2838633909	8.0369414608
H42	2.9848185072	8.3469996778	6.3667845755
H43	4.2494893409	8.6931436075	5.1881267987
H44	2.7570968008	6.6183823501	8.8368076599
H45	0.9929988466	6.5505280922	8.9473538043
H46	-0.3931439547	5.7357065069	7.0190538727
H47	0.3451326359	4.8143354163	5.6850734009
H48	0.5333175744	6.5602722751	5.7440254178
H49	2.9893301600	-0.2532071300	1.4514028642
C50	4.7772486156	-1.0020080947	2.3571775763
H51	4.8115775786	2.9128770296	0.7846374427
H52	4.0638970855	4.0490635246	-0.3520036803
H53	2.2765946998	2.4408149823	-1.1094936634
H54	1.3449541163	1.4929469720	0.0568173483
H55	3.0875069804	1.2019486893	-0.1497396529
H56	-0.3526242101	0.0484421913	3.1206511721
H57	1.3752632290	-0.3253710817	3.2152734845
H58	0.6472411627	0.1689234736	1.6717102536
H59	-0.2498215668	2.6165359090	1.4197531943
H60	-0.0751673954	3.7514356905	2.7725966727
H61	-1.1910006141	2.3709110488	2.8952628142
C62	5.6565827451	2.0944250476	8.6836328271
H63	6.1660348015	1.2370492977	6.7850421688
C64	5.8081803867	-0.7650681901	3.2632944394
H65	6.6651557538	0.6146595713	4.6618147897
H66	4.9819136675	3.1494274536	10.4366739154
H67	4.7500207058	-1.9310479896	1.7916598334
H68	6.2001955075	1.3411624366	9.2504111752
H69	6.5901584392	-1.5080829976	3.4054388705